THE ASTROPHYSICAL JOURNAL, 482:470–489, 1997 June 10

OPTICAL SPECTROSCOPY OF EZ CANIS MAJORIS: INDICATION FOR LARGE-SCALE STRUCTURES IN A WOLF-RAYET WIND

THIERRY MOREL,[1,2] NICOLE ST-LOUIS,[1] AND SERGEY V. MARCHENKO[1,2,3]
Received 1996 August 19; accepted 1997 January 9

ABSTRACT

We have carried out optical spectroscopy of the Wolf-Rayet star EZ CMa during 20 consecutive nights in 1995 January in support of the *IUE* Mega-project. In parallel with this optical spectroscopy, we also monitored EZ CMa using narrowband photometry. The light curve was found to be remarkably stable when folded with the $\mathscr{P} = 3.77$ day period, and it had a peak-to-valley amplitude of 0.1 mag.

The P Cygni absorption components of He I λ3889 and He I λ5876 display a similar global pattern of variability as was found for the simultaneously acquired UV profiles. The strengthening of the P Cygni absorption component of these transitions is associated with the maximum of the continuum flux. Conversely, the absorption trough of N V λ4604 gradually disappears as the star brightens. Although the emission parts of the lines are variable at different levels, they all show the same pattern of variability, which consists of phase-dependent shifts of extra emission components superposed on the profiles.

A strong correlation is found between the continuum-light level and the equivalent width of most transitions. The line skewness and the full-width at half-maximum show a daily recurrence timescale, reflecting the light curve changes. We have addressed in a rigorous statistical way the significance of the variations by calculating the "temporal variance spectrum." For any given line, we found enhanced variability at some velocities, although the whole profile displays a statistically significant level of variability.

Arguments against a compact companion as the cause of the observed periodic variability are presented. Instead, our observations strongly support the suggestion in the *IUE* Mega analysis that the atypical level of variability results from the rotation of a structured wind. We propose that the wind variability of EZ CMa is triggered by photospheric activity, or that the wind is controlled by a large-scale magnetic field.

Subject headings: stars: individual (EZ Canis Majoris) — stars: mass loss — stars: Wolf-Rayet — ultraviolet: stars

1. INTRODUCTION

With the advent of modern detectors and the launch of various space observatories, the observations of early-type stars have increased dramatically, both in quantity and quality. Spectroscopic observations of such stars on a sufficiently long temporal baseline often reveal a high level of spectral variability. In fact, this phenomenon is so common among OB stars, that spectral variability is now widely recognized as one of their fundamental properties.

Intensive spectroscopic monitoring is therefore a powerful tool to collect fundamental information about the physical processes operating in their envelope and to derive the basic properties of the star itself (e.g., Henrichs 1995; Fullerton, Gies, & Bolton 1996). Wolf-Rayet (WR) stars are no exception, displaying time-dependent spectroscopic variations, frequently accompanied by changes in photometry and polarimetry. The line-profile variations (*lpv*) can be schematically subdivided into two types: (a) Small, stochastic emission peaks of various sizes moving across the optical emission lines away from the line center, which are often attributed to local inhomogeneities in the wind carried out by the global stellar outflow (Moffat et al. 1988; Robert 1992); (b) large-scale spectral variations simultaneously affecting a significant part of the profile (e.g., McCandliss et al. 1994).

A periodic pattern in the line-profile and photometric variability has generally been found for the stars showing the latter type of behavior. Thereby, binary modulation was naturally suggested as the cause of the observed variability, with the secondary being a compact object (neutron star or black hole; hereafter *c*). Indeed, these objects are single-lined, which precludes the presence of a bright OB companion. Furthermore, the existence of WR + *c* systems is predicted by the general theory of massive close binary evolution (van den Heuvel & de Loore 1973; Tutukov & Yungelson 1973; Vanbeveren 1991), although the theoretically expected number is very low (De Donder, Vanbeveren, & van Bever 1997). On the other hand, since the timescale of the variability is comparable with the expected rotation period (a few days), rotational modulation of an inhomogeneous wind has also been suggested to account for the periodic *lpv*.

The interest in these single-line WR stars showing periodic variations is twofold: (a) An observational constraint for the evolutionary model of massive close binaries comes from the scarcity of WR + *c* systems discovered so far, the only unmistakably confirmed one being the strong X-ray emitter Cygnus X-3 (van Kerkwijk et al. 1996). Therefore, the identification of additional systems would be of considerable interest. (b) Rotational modulation persisting

[1] Département de Physique, Université de Montréal, C.P. 6128, Succ. Centre Ville, Montréal, Québec, H3C 3J7, Canada; and Observatoire du Mont Mégantic.

[2] Visiting Astronomer, University of Toronto Southern Observatory, Las Campanas, Chile.

[3] Visiting Astronomer, Cerro Tololo Inter-American Observatory, National Optical Astronomy Observatories, operated by the Association of Universities for Research in Astronomy, Inc., under cooperative agreement with the National Science Foundation; morel@astro.umontreal.ca, stlouis@astro.umontreal.ca, sergey@astro.umontreal.ca.

during several cycles would be a strong indication of the existence of a "wind-photosphere connection" in the form of (non)radial pulsations or magnetic fields controlling the wind morphology and dynamics. Because time-resolved, high-quality observations are required, the search for WR + c systems is severely biased toward the apparently brightest objects and is therefore far from complete (see Cherepashchuk & Aslanov 1984 for the latest review).

Among the single-lined WR stars with periodic variations, the WN 5 star EZ CMa (WR 6; HD 50896) exhibits the most striking variations. Along with its firmly established periodic nature ($\mathscr{P} = 3.77$ days), it is usually considered as the most promising WR + c candidate. As a suspected high-mass X-ray binary (HMXRB), EZ CMa was monitored in the soft X-ray spectral domain (<5 keV) by the *Einstein* and *ROSAT* observatories. Despite the paucity of the data, the X-ray flux was found to be variable on different timescales: from an hour (White & Long 1986), to a day (Willis et al. 1994). However, the nature of this X-ray variability is far from being completely clarified. In particular, Pollock (1989) criticized the statistical significance of the proposed hourly changes. Furthermore, whereas the *Einstein* observations showed a significant phase-modulation (Moffat et al. 1982), this is not apparent in the recent *ROSAT* data (Willis et al. 1994). Presumably, the observations are subject to strong epoch-dependency, just as was found for the optical light curve and UV spectroscopic changes (see below).

The first visual photometric variability of this object was reported by Ross (1961). Subsequent observations established the periodic nature of the light variations, as well as its incoherence over several cycles (Firmani et al. 1980), a result that has been confirmed by all recent investigations (Duijsens et al. 1996, and references therein). Despite the various shapes of the light curves, the variations (if any) are always phased with the 3.77 day period. Likewise, the polarimetric curves share this epoch-dependency (Robert et al. 1992).

EZ CMa was chosen as an *IUE* target on several occasions. The first UV-line-profile variability was reported by Willis et al. (1986). During the first long-term monitoring of this star (seven consecutive days in 1983), Willis et al. (1989) noticed a reduced level of variability compared with some archival spectra, as well as smaller continuum-flux variations. The changes occurred mainly in the extreme blue edge of the P Cygni absorption troughs, i.e., at or above the terminal velocity of the unperturbed wind. In an attempt to reveal the presence of a compact companion, the authors searched for evidence of the so-called "Hatchett-McCray effect" (Hatchett & McCray 1977). Basically, the presence of a compact companion orbiting within the dense stellar wind will result in a drastic increase of the ionization state of the material in its vicinity. This will lead to the formation of an X-ray photoionization zone, where the radiative force will be quenched (Blondin 1994). Since the wind of WR stars is assumed to be radiatively driven, the dynamics in this region will be seriously altered. This can lead to a number of directly observed effects: (a) Reduction of the wind terminal velocity during the passage of the compact companion in front of the WR component; (b) phase-dependent variations of the emission part of the profiles caused by the orbital revolution of the wind cavity around the WR star. The Hatchett-McCray effect was observed in some HMXRBs (e.g., Kaper, Hammerschlag-Hensberge, & van Loon 1993). Since this search was inconclusive for EZ CMa (albeit a tentative phase-dependent variability with a 1 day timescale was reported), the observed UV changes were ascribed to be intrinsic to the WR wind. A follow-up study based on a 6 day run in 1988 (St-Louis et al. 1993) showed a somewhat higher degree of activity, but nevertheless confirmed the conclusions of Willis et al. (1989), notably the existence of the 1 day recurrence timescale. Because the variations in the absorption and emission components of the major UV P Cygni profiles were not correlated, the linear extension of the material causing the changes was estimated to be of the order of the WR core radius. A different pattern of variability was observed in 1992 (St-Louis 1994; St-Louis et al. 1997). The phase-dependent appearance of an excess in P Cygni absorption at high negative velocities ($v \geq 2000$ km s^{-1}) was accompanied by a reduced absorption at intermediate negative velocities ($1800 > v > 1000$ km s^{-1}). This can also be seen in the 1995 UV observations (St-Louis et al. 1995, hereafter WRMEGA). The variability was interpreted as a rotationally induced crossing in the line of sight of faster and hotter regions of the wind.

The most comprehensive optical spectroscopic study secured so far (Firmani et al. 1980) provided the first evidence for the periodic nature of the *lpv*. The observed phase-dependent variations were attributed to the disturbance of the stellar wind by an orbiting companion. The very low mass-function derived from the radial velocity perturbations [$f(M) \sim 0.015\ M_\odot$], combined with a polarization estimation of the orbital inclination (McLean et al. 1979), led to a mass of the secondary typical of a neutron star: $1.32 \pm 0.15\ M_\odot$. Ebbets (1979) also favored the binary hypothesis with the same conclusion regarding the nature of the secondary. This view was later supported by the detection of high-velocity interstellar lines in the high-resolution spectra of EZ CMa, which were interpreted as revealing the existence of an old supernova remnant in the line of sight of this WR star (Howarth & Phillips 1986; Nichols-Bohlin & Fesen 1986). However, the possibility of a direct association is not proven yet, mainly owing to the controversial distance to EZ CMa (Howarth & Phillips 1986; Nichols & Fesen 1994). Thereafter, a growing number of studies have questioned the existence of a compact companion, since the radial velocity variations that are supposed to describe a hypothetical binary motion can easily be introduced by large-scale *lpv* (e.g., Robert et al. 1992; St-Louis et al. 1993). An alternative approach was proposed by Underhill & Yang (1991), who interpreted the observed *lpv* as a rotational modulation of a ringlike disk connected to the central star by ever-changing filaments.

Despite the wealth of optical spectroscopic data already collected, an investigation based on an intensive time-resolved data set taking advantage of the capacities of modern detectors was still lacking. The *IUE* MEGA campaign (Massa et al. 1995) provided a unique opportunity to carry out such a study, with 16 contiguous days of observation of three early-type stars: ζ Pup (O4 If(n)), HD 64760 (B0.5 Ib) and EZ CMa. For the latter, preliminary results were presented in WRMEGA. Simultaneously with this campaign, we have obtained an extensive set of optical spectroscopy and photometry, which will be discussed in this article.

The data acquisition and the reduction procedure will be presented in § 2; § 3 will summarize our photometric (§ 3.1)

TABLE 1

NARROWBAND PHOTOMETRY OF EZ CMA IN 1995

HJD −2440000	Phase	u(W-R–c1)	u(c2–c1)	v(W-R–c1)	v(c2–c1)	Rapid Photometry
9730.5864	0.808	−0.594	0.362	0.790	0.310	...
9730.6965	0.837	−0.605	0.349	0.785	0.304	
9730.7655	0.855	−0.602	0.360	0.770	0.303	
9730.8171	0.869	...	...	0.778	0.301	
9732.5952	0.341	−0.663	0.349	0.721	0.306	...
9732.6829	0.364	−0.673	0.351	0.723	0.313	
9732.8557	0.410	−0.648	0.354	0.740	0.305	
9733.6656	0.625	−0.561	0.352	0.822	0.306	...
9733.7450	0.647	−0.574	0.353	0.809	0.308	
9733.8308	0.669	−0.578	0.352	0.806	0.298	
9734.5461	0.859	−0.622	0.356	0.768	0.307	1
9734.6280	0.881	−0.634	0.357	0.758	0.307	
9734.7792	0.921	−0.620	0.348	0.756	0.302	
9734.8225	0.933	−0.611	0.357	0.774	0.313	
9735.5551	0.127	−0.699	0.346	0.721	0.302	1
9735.6195	0.144	−0.688	0.351	0.705	0.307	
9735.6750	0.159	−0.690	0.347	0.706	0.304	
9735.7328	0.174	−0.692	0.348	0.702	0.304	
9735.8059	0.194	−0.680	0.338	0.714	0.309	
9735.8474	0.205	−0.674	0.361	0.714	0.305	
9736.5702	0.397	−0.653	0.355	0.732	0.300	2
9736.6239	0.411	−0.660	0.349	0.733	0.310	
9736.7108	0.434	−0.648	0.353	0.738	0.300	
9736.7777	0.452	−0.634	0.358	0.750	0.302	
9736.8095	0.460	−0.640	0.348	0.747	0.304	
9736.8472	0.470	−0.632	0.347	0.754	0.305	
9737.5537	0.658	−0.602	0.352	0.794	0.299	2
9737.6080	0.672	−0.591	0.357	0.797	0.315	
9737.6970	0.696	−0.595	0.347	0.793	0.315	
9737.7631	0.713	−0.591	0.353	0.798	0.310	
9737.7962	0.722	−0.594	0.356	0.790	0.306	
9737.8223	0.729	−0.588	0.352	0.785	0.308	
9738.5516	0.923	−0.614	0.351	0.774	0.303	2
9738.6087	0.938	−0.612	0.353	0.776	0.311	
9738.6972	0.961	−0.595	0.350	0.786	0.312	
9738.7564	0.977	−0.597	0.349	0.792	0.309	
9738.7872	0.985	−0.592	0.351	0.793	0.307	
9738.8195	0.994	−0.593	0.350	0.791	0.316	
9738.8506	0.002	−0.604	0.354	0.784	0.310	
9739.5510	0.188	−0.675	0.350	0.718	0.304	2
9739.6063	0.203	−0.671	0.353	0.720	0.311	
9739.6918	0.226	−0.662	0.349	0.733	0.307	
9739.7538	0.242	−0.653	0.351	0.734	0.304	
9739.7846	0.250	−0.664	0.356	0.725	0.309	
9739.8133	0.258	−0.659	0.352	0.728	0.311	
9739.8535	0.269	−0.649	0.356	0.729	0.305	
9740.5700	0.459	−0.644	0.363	0.735	0.309	...
9740.6046	0.468	−0.637	0.341	0.741	0.311	
9740.6562	0.482	−0.626	0.351	0.760	0.308	
9741.5515	0.720	−0.592	0.354	0.785	0.308	1
9741.5877	0.729	−0.600	0.350	0.787	0.303	
9741.6200	0.737	−0.599	0.351	0.783	0.307	
9741.6513	0.746	−0.604	0.344	0.782	0.310	
9741.7075	0.761	−0.605	0.358	0.772	0.310	
9741.7679	0.777	−0.604	0.350	0.784	0.310	
9741.7977	0.785	−0.602	0.350	0.784	0.312	
9741.8260	0.792	−0.597	0.357	0.784	0.308	
9742.5518	0.985	−0.590	0.352	0.799	0.312	2
9742.6006	0.998	−0.590	0.355	0.794	0.306	
9742.6791	0.019	−0.601	0.349	0.785	0.312	
9742.7104	0.027	−0.609	0.353	0.778	0.306	
9742.7681	0.042	−0.610	0.348	0.780	0.309	
9742.7986	0.051	−0.628	0.341	0.767	0.306	
9742.8274	0.058	−0.626	0.350	0.764	0.305	
9743.5456	0.249	−0.658	0.361	0.738	0.310	2
9743.5955	0.262	−0.659	0.355	0.728	0.305	
9743.6495	0.276	−0.660	0.352	0.732	0.312	
9743.7026	0.291	−0.652	0.349	0.738	0.311	
9743.7255	0.297	−0.660	0.348	0.738	0.306	
9743.7804	0.311	−0.663	0.347	0.725	0.308	
9743.8107	0.319	−0.669	0.357	0.727	0.309	
9743.8414	0.327	−0.658	0.345	0.727	0.308	
9744.5517	0.516	−0.592	0.348	0.782	0.300	2

TABLE 1—*Continued*

HJD −2440000	Phase	*u*(W-R–c1)	*u*(c2–c1)	*v*(W-R–c1)	*v*(c2–c1)	Rapid Photometry
9744.6008.....	0.529	−0.588	0.361	0.798	0.307	
9744.6535.....	0.543	−0.584	0.349	0.798	0.305	
9744.7074.....	0.557	−0.590	0.339	0.803	0.313	
9744.7600.....	0.571	−0.585	0.346	...	0.309	
9744.7885.....	0.579	−0.601	0.344	0.806	0.309	
9744.8148.....	0.586	−0.587	0.351	0.788	0.315	
9744.8420.....	0.593	−0.607	0.343	0.787	0.309	
9745.5512.....	0.781	−0.591	0.353	0.794	0.307	2
9745.5987.....	0.794	−0.599	0.354	0.790	0.309	
9745.6523.....	0.808	−0.598	0.352	0.782	0.310	
9745.7049.....	0.822	−0.595	0.357	0.797	0.305	
9745.7591.....	0.837	−0.607	0.359	0.784	0.307	
9745.7865.....	0.844	−0.605	0.354	0.784	0.308	
9745.8124.....	0.851	−0.613	0.349	0.778	0.315	
9745.8387.....	0.858	−0.610	0.351	0.777	0.310	
9746.5583.....	0.049	−0.624	0.351	0.769	0.308	1
9746.6089.....	0.062	−0.633	0.345	0.755	0.301	
9746.6536.....	0.074	−0.648	0.348	0.750	0.311	
9746.7076.....	0.089	−0.659	0.353	0.738	0.314	
9746.8162.....	0.117	−0.678	0.347	0.719	0.310	
9747.5841.....	0.321	−0.656	0.362	0.737	0.313	1
9747.6388.....	0.336	−0.660	0.354	0.735	0.311	
9747.7242.....	0.358	−0.662	0.351	0.738	0.309	
9747.8227.....	0.384	−0.671	0.361	0.731	0.308	
9748.5760.....	0.585	−0.585	0.353	0.793	0.307	...
9748.6332.....	0.600	−0.597	0.354	0.789	0.302	
9748.7168.....	0.622	−0.606	0.349	0.790	0.310	
9748.7629.....	0.634	−0.591	0.349	0.797	0.311	
9748.8137.....	0.648	...	0.348	0.804	0.310	
9749.6736.....	0.876	−0.637	0.355	0.770	0.311	2
9749.7257.....	0.890	−0.618	0.351	0.773	0.307	
9749.7946.....	0.908	−0.609	0.354	0.773	0.301	

and spectroscopic results (§ 3.2). The possible duplicity of EZ CMa will be discussed in § 4.1, while § 4.2 will be devoted to an interpretation of the observed variability as rotationally induced. We will discuss the possible existence of localized or large-scale magnetic structures in § 4.3. Finally, our main conclusions will be given in § 5.

2. OBSERVATIONS AND REDUCTION PROCEDURE

2.1. *Photometry*

Our photometric data were obtained with the one-channel photometer of the 60 cm Lowell telescope at CTIO (S-20 phototube and cold box 57). In an attempt to follow any possible color variations in the continuum of EZ CMa, two narrowband filters were chosen: one with central wavelength $\lambda_0 = 3650$ Å and full width at half-maximum FWHM = 100 Å (*u* filter), and the other with $\lambda_0 = 5140$ Å and FWHM = 90 Å (*v* filter), the latter being the same as used during the three-month monitoring campaign in 1993 (Antokhin et al. 1994). Note that these filters are very close to the continuum (*u*, *v*) WR filters used by Smith (1968). We used "traditional" comparison stars, c1 = HD 50853 and c2 = HD 50711, in the following sequence of 15 s integrations through an 18″ or 25″ diaphragm: sky(*u*, *v*)–c2(*u*, *v*)–c1(*u*, *v*)–WR(*u*, *v*)–c1(*u*, *v*)–WR(*u*, *v*)–c1(*u*, *v*)–c2(*u*, *v*)–sky(*u*, *v*). The data were reduced using the extinction coefficients derived from observations of all available comparison stars: we have followed three additional objects, HD 5980, HD 64760, and HD 66811. We applied two sets of extinction coefficients: $k_u = 0.466$, $k_v = 0.137$ before 26/27 1995 January, and $k_u = 0.565$, $k_v = 0.203$ afterward. The journal of observations (Table 1) gives the heliocentric Julian dates (HJD), the phases, and the *u* and *v* magnitudes. The phases, as everywhere in this paper, were calculated according to the ephemeris of Lamontagne, Moffat, & Lamarre (1986). The overall (c2–c1) accuracy was: $\sigma(u) = 0.0049$ mag and $\sigma(v) = 0.0039$ mag.

In an attempt to confirm the short period, $\mathscr{P} \sim 0.11$ s, announced as a result of five nights of rapid photometry of EZ CMa in 1993 (Marchenko et al. 1994), we have obtained a significantly larger data set, comprising observations 1–2 times per night in the broadband *V* filter, with 0.02 s time resolution. Every ∼10 minute record of EZ CMa was immediately followed by the same length record of the comparison star c1 to complete one cycle of fast photometry. In the "fast photometry" column of Table 1 the number of complete cycles is listed for each night. For a given night, two cycles were separated by a 2–4 hr interval.

2.2. *Spectroscopy*

Spectroscopic observations were secured in the interval 1995 January 10–29 at the 60 cm Helen Sawyer-Hogg telescope at the Las Campanas Observatory in Chile. The spectrograph was equipped with a Photometrics PM 512 chip.

In order to obtain a good compromise between resolution and spectral coverage, we selected the 600 lines mm^{-1} diffraction grating blazed at 4700 Å in the first order, which gives 2.2 Å $pixel^{-1}$ reciprocal dispersion. We observed EZ CMa over a wide spectral domain in order to characterize the *lpv* for lines with a broad range of excitation potential, i.e., to probe different line-formation regions. Accordingly, our spectra cover the following regions: 3700–4800 Å, 4450–5550 Å, and 5650–6750 Å. Three consecutive exposures (with unit exposure time ranging from about 50 s in the blue to 120 s in the yellow region) were combined to

improve the signal-to-noise ratio, which is typically around 100 in the continuum of the net spectrum. We eliminated any spectrum showing a deviation obviously attributable to an inadequate rectification procedure or saturated exposures. This resulted in 85, 99 and 62 spectra for each spectral domain, respectively. We did not find any significant short-term (below 5 minutes) variability while grouping the exposures.

The standard reduction procedure (i.e., bias subtraction, flat-fielding, removal of cosmic rays, extraction of the spectra and wavelength calibration) was carried out using IRAF[4] reduction packages. The calibration lamp spectra were taken systematically before the star exposure in order to avoid any flexure problems. We used an argon lamp for the first two spectral regions and a neon lamp for the last one. Since we intended to characterize changes in the line profiles, which are often of the order of a few percent, the rectification of the spectra was one of the most crucial steps in the reduction procedure. We have carefully selected five to seven fixed wavelength continuum regions for each spectral domain, with an extent varying from 4 to 112 Å, and we have fitted the continuum with a Legendre polynomial of the fifth or sixth order.

We used the light curve to eliminate the variability induced by the continuum-light modulation in the following way: First we binned the light curve to 0.01 phase resolution. Then we multiplied all the rectified spectra in accordance to their phase ϕ by $10^{-0.4[m_v(\phi)-m_v(\min)]}$, where $m_v(\phi)$ and $m_v(\min)$ are the magnitudes for a given phase ϕ and at minimum light, respectively. The constant continuum level was subtracted before, and added back in after this procedure. Therefore, the remaining variations should be entirely attributable to the emission lines.

3. RESULTS

3.1. *Photometry*

In Figure 1 we plot the light curve of EZ CMa folded with the $\mathscr{P} = 3.77$ day period. Because of the extremely small amplitude of the $u - v$ color variations, we plot only the v filter data (*filled dots*). The light curve covers five complete cycles. Its small (for a fixed phase) scatter indicates that, during our observations, the 3.77 day periodicity completely dominated the shape of the light curve. Open symbols (*middle panel*) denote the value $2.5 \times \log [F(\lambda_1) + F(\lambda_2)]$, where the wavelengths $\lambda_1 = (1689 \pm 9)$ Å and $\lambda_2 = (1860 \pm 40)$ Å are continuum-dominated regions in the *IUE* spectrum of EZ CMa. This far-ultraviolet light curve was shifted by a constant value to match the minimum (phases 0.5–0.8) in v light. It is clear that the amplitude increases toward the far ultraviolet. This, along with the fact that the P Cygni absorption component of N v λ4604 disappears at $\phi = 0.1$–0.5 (§ 3.2.2), strongly suggests that the temperature at the base of the wind of EZ CMa increases during maximum light.

Inspired by the positive detection of a short, $\mathscr{P} \sim 0.11$ s ($f = 9.048$ Hz), period during V-band photometric observations in 1993 (Marchenko et al. 1994), which could be related to the rapid rotation of a neutron star, we performed a more systematic search in 1995. All the $\sim$10 minute

[4] IRAF is distributed by the National Optical Astronomy Observatories, operated by the Association of Universities for Research in Astronomy, Inc., under cooperative agreement with the National Science Foundation.

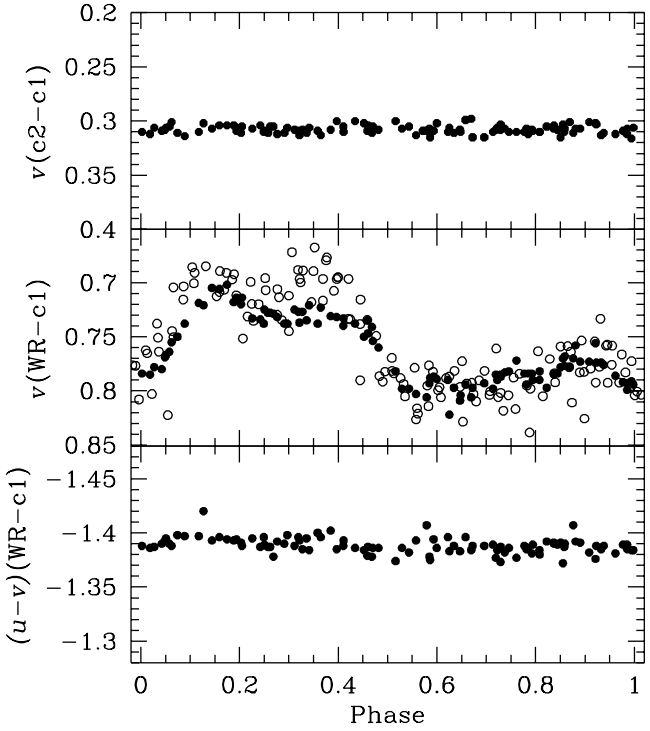

FIG. 1.—Light curve of EZ CMa. *Upper panel*: differential v magnitudes for the c1 and c2 comparison stars. *Central panel*: v filter light curve (*filled dots*); combined *IUE* continuum (*open symbols*; see text). *Bottom panel*: $u - v$ color variations.

records (around 3×10^4 data bins, 0.02 s each) of EZ CMa and the comparison star were Fourier-transformed to create a mean power spectrum (MPS) of the whole run: a total of 23 records for EZ CMa and 21 records of the comparison star. The MPS of EZ CMa appeared to be featureless when applying the 1% or 0.5% detectability thresholds (Bendat & Piersol 1986; Marchenko et al. 1994).

Because the orbital parameters of the hypothetical neutron star are not known, any comprehensive search for periodic signals must allow for the Doppler shifts produced by orbital revolution. As a first approximation, we assumed a circular orbit. Hence, the search for periodicities was performed by varying K (the radial velocity amplitude) and the "zero" orbital phase of the compact companion (the moment when the companion passes in front of the WR star). We have chosen the grid: $K = 100$–600 km s^{-1} with 12.5 km s^{-1} steps, and orbital phases $\phi \sim = 0°$–$360°$ with 20°–15°–10° steps, the larger step applies to the smaller K.

The same procedure was applied to the 1993 data (nine records of EZ CMa). Note that this treatment, which is different from the one used in Marchenko et al. (1994), might slightly change the previously found frequencies (i.e., $f = 9.048$ Hz). There are some encouraging similarities between the 1993 and 1995 data sets. We found significant signals at:

$f = 1.094$ Hz (1993) and $f = 1.096$ Hz (1995) for $K = 300$ km s^{-1};
$f = 1.490$ Hz (1993) and $f = 1.487$ Hz (1995) for $K = 412$ km s^{-1};
$f = 1.714$ Hz (1993) and $f = 1.699$ Hz (1995) for $K = 588$ km s^{-1};
$f = 1.782$ Hz (1993) and $f = 1.796$ Hz (1995) for $K = 450$ km s^{-1};

$f = 2.649$ Hz (1993) and $f = 2.650$ Hz (1995) for $K = 450$ km s^{-1};
$f = 9.036$ Hz (1993) and $f = 9.038$ Hz (1995) for $K = 450$ km s^{-1}.

However, practically all the features in the combined spectrum are generated by the individual power spectrum of the record obtained at HJD 2449747.794 under unfavorable weather conditions. When it is removed from the 1995 data set, the combination of the remaining 22 power spectra produces a practically featureless MPS. This casts serious doubt on the significance of any 1993–1995 similarities.

3.2. *Spectroscopy*

3.2.1. *The Emission-line Variability*

3.2.1.1. The Morphological Behavior of the Spectral Lines

The high degree of activity observed in optical photometry and in the UV spectra (WRMEGA) is also reflected by our optical data set. The emission lines demonstrate a remarkable level of variability on an hourly timescale. The temporal behavior of these variations is strictly coherent over the five cycles covered by the observations. Excluding N v λ4945 (its subtle variations cannot be easily related to the *lpv* of other transitions), we found that the same variability pattern affects all the emission-line profiles with the possibility of small phase lags. Also, the variability of the He i λ5876 emission component is difficult to associate with that of other transitions since this line is severely blended with unresolved telluric and interstellar lines. The *degree* of variability, however, varies from one line to another. In particular, the characteristics of the helium line or C iv λ5806 *lpv* also apply to N iv λ4058, although the changes are more dramatic for the latter. The behavior of three lines, N iv λ4058, He ii λ6560 and N v λ4945, is displayed in Figure 2. The representative profiles resulting from 0.05-phase binning are compared with the mean template profile (*dashed line*). This template spectrum was constructed by giving an equal weight to every 0.05 bin, irrespective of the number of spectra in a given bin. The *lpv* of the helium lines often show recurrent structures with a timescale of about 1 day (see for example the similarity between the profiles at $\phi \sim 0.125$, 0.425 and 0.725), indicating that nearly the same wind state is encountered three times per cycle. Similarities are also found for profiles taken about $\phi \sim 0.2$ apart

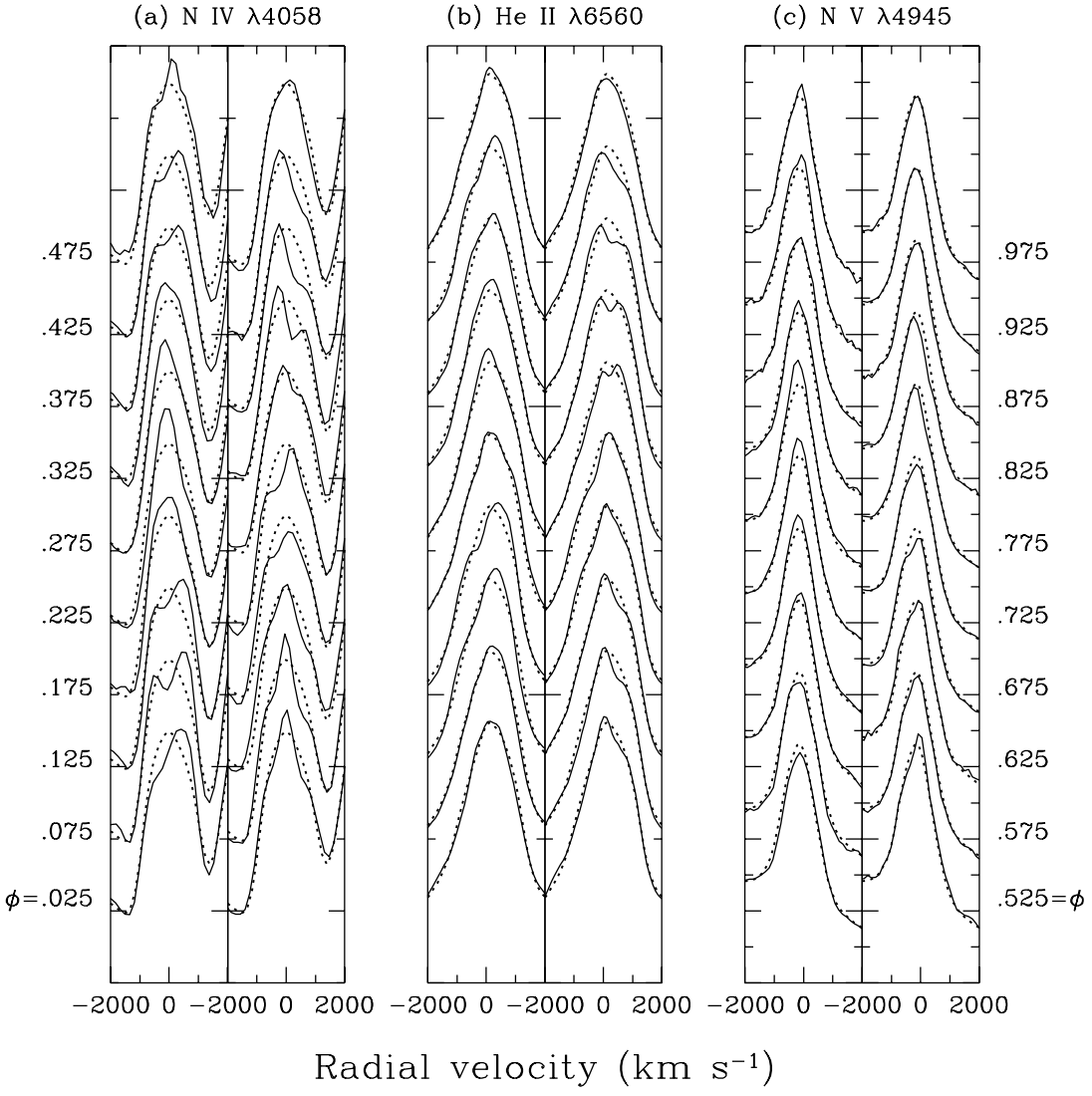

FIG. 2.—Time series of (*a*) N iv λ4058, (*b*) He ii λ6560, and (*c*) N v λ4945. The rectified spectra were binned to a 0.05 phase interval. The corresponding mean phases are indicated on both sides of this plot. The mean profile is overplotted as a dashed line. The intensities are in arbitrary units.

($\phi \sim 0.275$, 0.625 and 0.925). Finally, we note the appearance of a well-defined double-peaked profile at $\phi \sim 0.8$. The similarity of the *lpv* affecting all the transitions can readily be seen in Figure 3, where we present a gray-scale plot of the residuals from the mean profile for three selected lines: N IV λ4058, He II λ4686 and He II λ6560. The pattern of variability can be assimilated to various extra emission components waving around the line center. This complex behavior is somewhat similar to the one found (with a period of 2.27 days) in the He II transitions of the WN 6 star WR 134 (McCandliss et al. 1994). It is extremely difficult to follow consistently the motion of these individual extra emission features over the entire cycle. Although their motion is readily seen within the velocity range of about ± 1500 km s^{-1}, an extension of the variability to higher Doppler shifts is discernible up to at least ± 2000 km s^{-1} (Figs. 3*b* and 3*c*), which roughly corresponds to the value of the wind terminal velocity (~ 1900 km s^{-1}; Prinja, Barlow, & Howarth 1990; Rochowicz & Niedzielski 1995). The significance of these high-velocity changes will be rigorously demonstrated in § 3.2.3.

In order to investigate the dynamics of the extra emission features appearing in Figure 3, we have measured their radial velocity by determining the wavelength at which the total flux of the feature is divided into two equal parts. The results are presented in Figure 4 for He II λ6560. Since the emission lines probe the conditions of the wind averaged over the entire stellar envelope, it is likely that overlap in velocity space of different extra emission components, as well as opacity effects considerably complicate the observed pattern of variability. It is, however, remarkable that the *bluest* excursions of these substructures coincide with the occurrence of the brightness maxima at $\phi \sim 0.15$ and 0.40 (compare Figs. 1 and 4). In particular, no extra emission is observed at high negative velocities during minimum light ($\phi \sim 0.5$–0.8).

In order to quantify the nature of the variability displayed by all transitions at $v > +2000$ km s^{-1}, we have measured the wing intensity of He II λ4686 for a fixed wavelength (here 4719 Å, which corresponds to $v \sim +2140$ km s^{-1}; the red wing variability reaches a maximum at this velocity, see § 3.2.3). The results (Fig. 5) bear a striking similarity with the light curve and suggest a causal relationship. This variability could be partially related to the variations at negative-to-zero velocities brought to the positive domain by electron scattering (Hillier 1984, 1991). However,

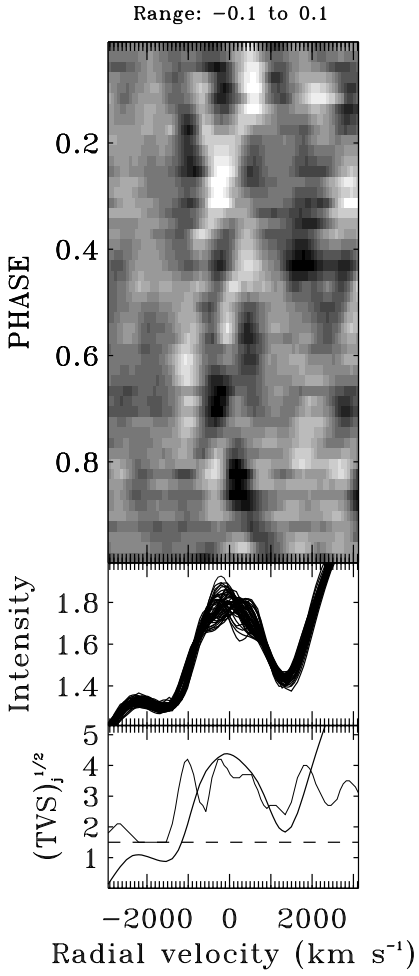

FIG. 3*a*

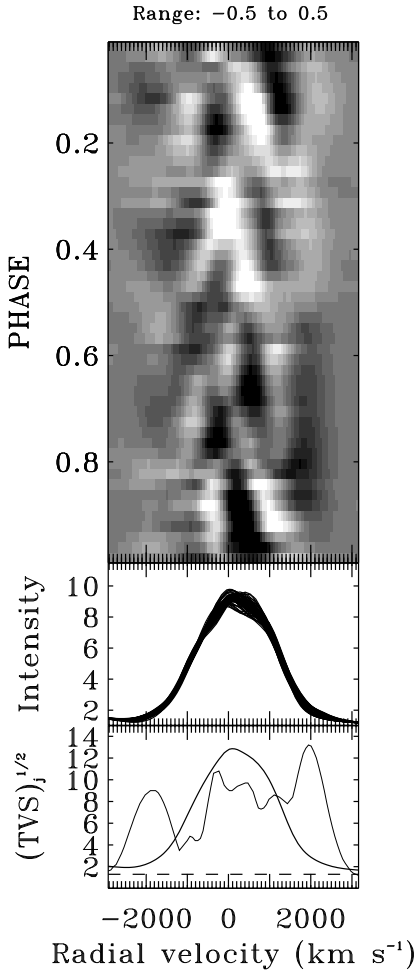

FIG. 3*b*

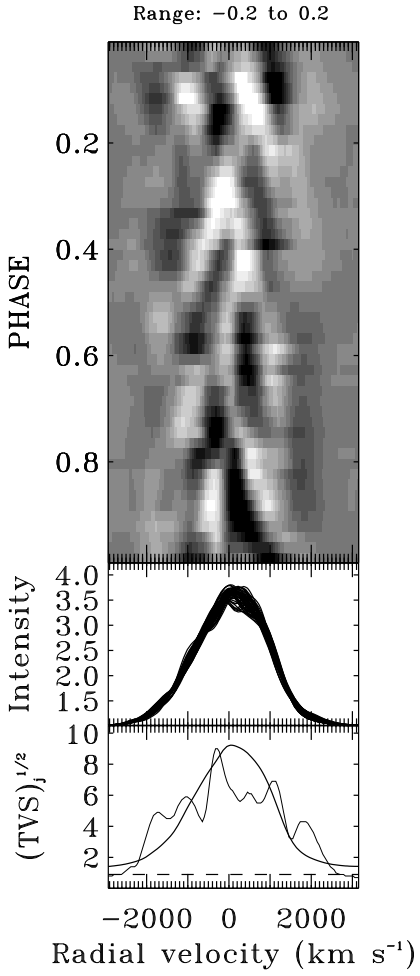

FIG. 3*c*

FIG. 3.—Gray-scale plot of the time series of the residuals of (*a*) N IV λ4058, (*b*) He II λ4686, and (*c*) He II λ6560. These residuals (the mean profile subtracted from the individual profiles) were binned to a 0.02 phase interval. An extra emission component appears brighter in these plots. The middle panel presents the superposition of the different rectified profiles. The values of $(\mathrm{TVS})_j^{1/2}$ (§ 3.2.3) and the mean profile (in arbitrary units) are presented in the lower panel. The horizontal dashed line indicates the 55% variability detection threshold. All velocities are heliocentric.

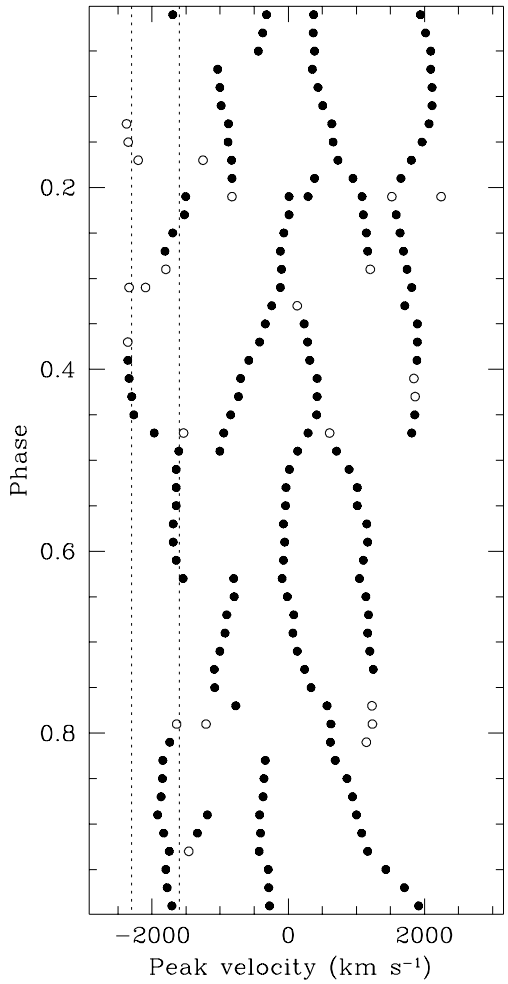

FIG. 4.—Estimation of the Doppler shifts (referred to the laboratory rest wavelength) associated with the different subpeaks traveling across the He II λ6560 profile. Measurements indicated with a black dot possess a higher degree of confidence. The dashed lines indicate the isovelocities −1600 and −2300 km s^{-1} (see text).

the relative amplitude of the variations at $v \sim +v_\infty$ exceeds the variations in the $-v_\infty$-0 domain (§ 3.2.3). In addition, there is a clear anticorrelation between the intensities measured at $+v_\infty$ and $-v_\infty$ (see § 4.1). Thus, these positive-velocity changes might reflect the genuine changes of the wind structure at $|v| \sim v_\infty$.

As mentioned previously, N V λ4945 does not display a high degree of variability. However, the *lpv* inherent in this line are significant (§ 3.2.3) and show some phase dependency (Fig. 6). The variability is mainly restricted to the uppermost part of the profile and seems to differ from the variations of the "typical" lines discussed above (compare Figs. 2*b* and 2*c* between $\phi \sim 0.525$ and 0.675). However, these differences do not clearly indicate that this line is not sensitive to the same time-dependent physical conditions as the other transitions. In particular, we note that the line-peak intensity is also enhanced at $\phi \sim 0.3$.

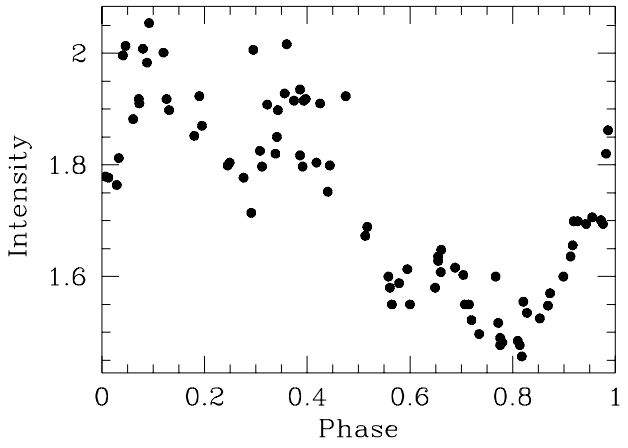

FIG. 5.—Red-wing intensity of He II λ4686 measured at 4719 Å

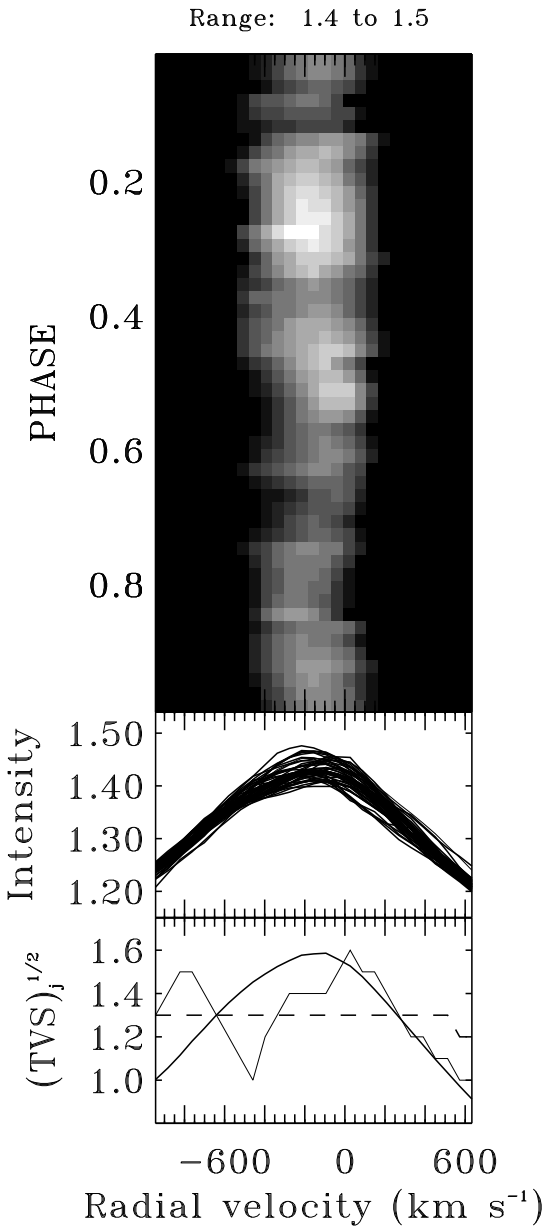

FIG. 6.—Gray-scale plot of the time series of N V λ4945. The rectified spectra were binned to a 0.02 phase interval. The middle panel presents the superposition of the different rectified profiles. The value of $(TVS)_j^{1/2}$ (§ 3.2.3) and the mean profile (in arbitrary units) are presented in the lower panel. The horizontal dashed line indicates the 55% variability detection threshold. All velocities are heliocentric.

3.2.1.2. Equivalent Width Variations

For each line, we have measured the equivalent width (EW) within a fixed wavelength range. As much as possible, this range was chosen in order to minimize the contribution of blends. The results (which were normalized for comparison) are shown for six selected lines in Figure 7. Note that the plotted variations reflect the net changes of emissivity after allowance for the continuum level changes. The EW variations reach a maximum value (20%) for He II λ4542 and N V $\lambda\lambda$4604, 4620. Lower level changes are detected in He II λ4686 and N IV λ4058, while the variations observed in other lines (such as He II λ4200 or N V λ4945) are comparable with the measurement errors.

In Figure 8, the line profiles corresponding to the maximum and minimum EW values are plotted for four transitions. The different responses to a change in the physical conditions are noticeable for the two Pickering lines He II λ4200 and He II λ4542. Since He II λ4542 is blended with multiple lines of N III around 4513 Å, we were compelled to restrict our measurements to the region 4526–4578 Å. Even if we account for a possible distinct behavior of the N III transitions, it seems unlikely that the amplitude of the EW variations can decrease sufficiently to remove the observed difference. As a possible explanation of this peculiarity one can invoke the argument of Conti, Leep, & Perry (1983): this line might be at the verge of the optically thick/thin case, exposing particular sensitivity to the variations of the continuum flux.

In the case of the doublet N V $\lambda\lambda$4604, 4620, the high amplitude of the observed EW variations can mostly be explained by the appearance and disappearance of the P Cygni absorption components (§ 3.2.2). According to Hillier (1988), collisional excitation is an important process in the formation of these lines. Therefore, they must be highly sensitive to the temperature fluctuations occurring at the base of the wind (Fig. 1), i.e., in the vicinity of the line formation zone (this doublet is formed at $\sim 3\ R_c$, where R_c is the stellar core radius; P. Crowther 1995, private communication). As far as the lines exhibiting the largest changes are concerned, the equivalent width variations are strongly correlated with the continuum flux level: the equivalent width decreases as the star fades

3.2.1.3. Skewness Variations

In order to quantify the phase-related changes in the line asymmetry (Fig. 2), we have calculated the skewness of the line profiles:

$$\beta^{1/2} = \mu_3/\mu_2^{3/2} ,$$

where

$$\mu_n = \sum_j (\lambda_j - \bar{\lambda})^n I_j / \sum_j I_j ,$$

and

$$\bar{\lambda} = \sum_j \lambda_j I_j / \sum_j I_j .$$

Here, I_j is the intensity of the line at the wavelength λ_j. We have measured the skewness above a given intensity in order to avoid the blended part of the profile. The results are plotted in Figure 9 for four selected transitions. The 1 day recurrence timescale inferred visually (§ 3.2.1.1) appears clearly for most of the lines (e.g., He II λ4686), excluding N V λ4945. This result is reminiscent of the 1 day recurrence timescale found in the EW of the UV absorption components by Willis et al. (1989) and St-Louis et al. (1993). No comparative information can be gained from these data since, for a given transition, both the amplitude and the shape of the curves depend on the chosen intensity level above which the skewness value was determined (compare the values of Figs. 9 and 10 for He II λ4686 and He II λ6560).

3.2.1.4. Radial Velocity Variations

Because most of the optical lines of EZ CMa are blended and asymmetric, the difficulties in the determination of

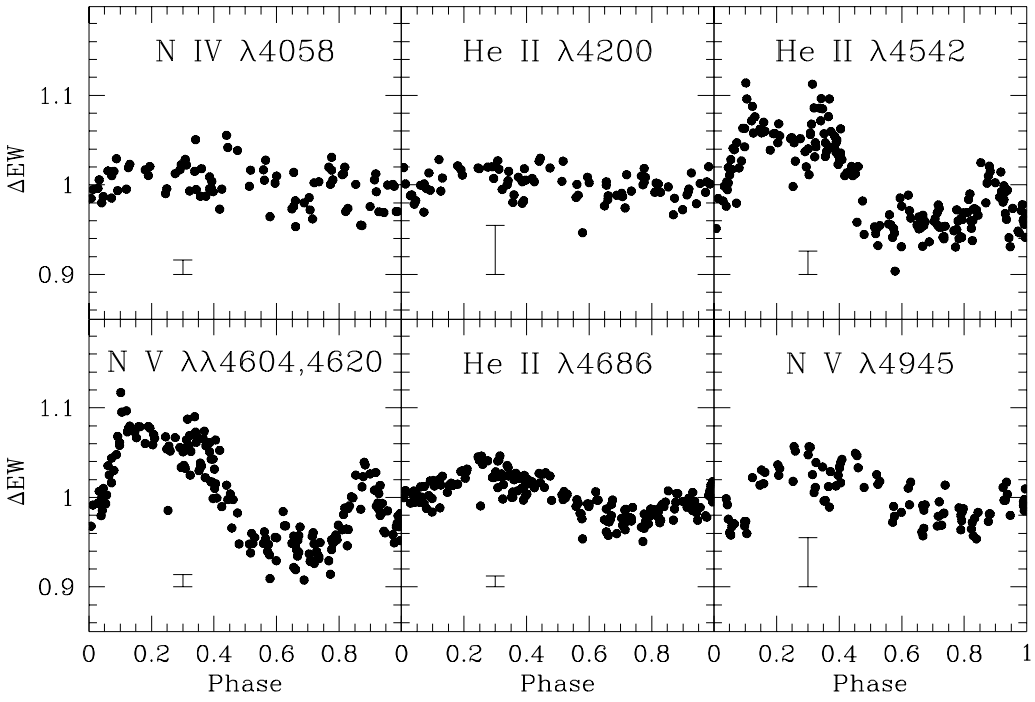

FIG. 7.—Equivalent widths (normalized to the mean value) of six selected transitions. The error bars (2 σ) were calculated according to Chalabaev & Maillard (1983).

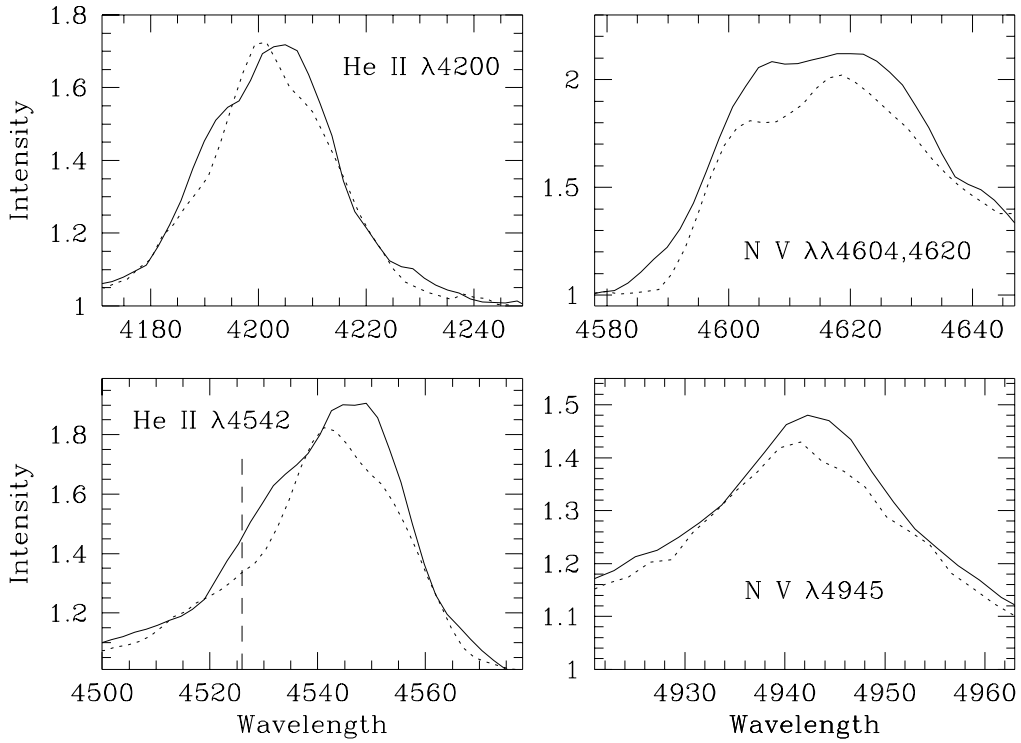

FIG. 8.—Comparison of the He II λ4200, He II λ4542, N V $\lambda\lambda$4604, 4620, and N V λ4945 profiles associated with the minimum (*dashed line*; $\phi \sim 0.579$ for the helium transitions, $\phi \sim 0.839$ for N V λ4945) and the maximum EW values (*solid line*; $\phi \sim 0.120$ for the helium transitions, $\phi \sim 0.256$ for N V λ4945). The wavelength range of these figures corresponds to the limits where the equivalent width measurements were performed (except for He II λ4542: longward of 4526 Å).

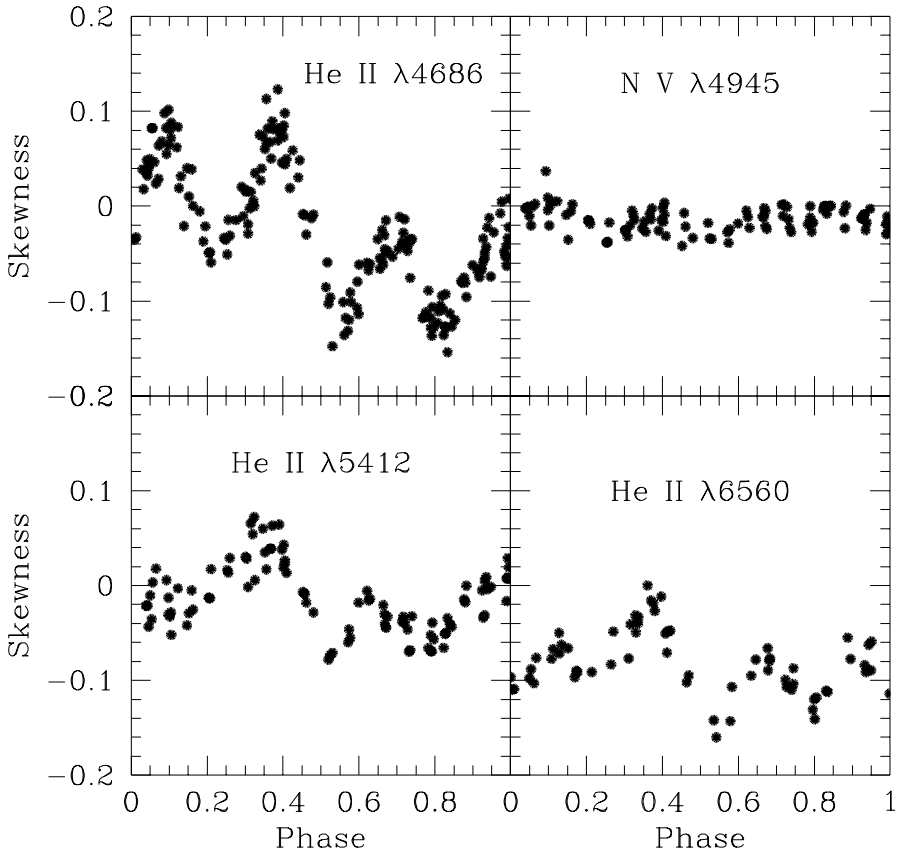

FIG. 9.—Skewness measurements for four selected transitions

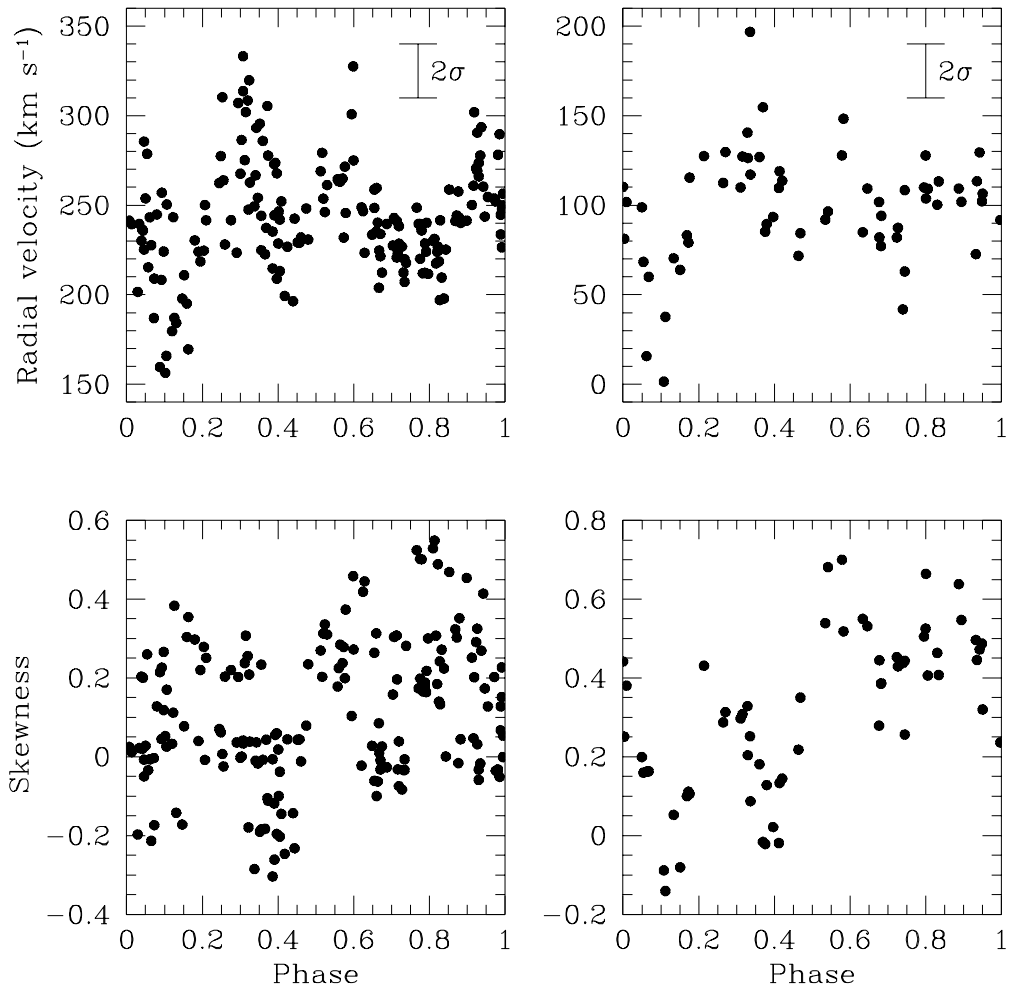

FIG. 10.—Comparison between the heliocentric radial velocities and the skewness measurements for He II λ4686 (*left panels*) and He II λ6560 (*right panels*). Both measurements were performed for the intensity ranges 3–6.5 and 1.35–2.5 for He II λ4686 and He II λ6560, respectively.

radial velocity variations are well known. The reliability of the results strongly depends on the method used as well as on its applicability range. Consequently, we excluded from our measurements the uppermost highly variable part of the profiles, which does not reflect in a straightforward manner (i.e., via orbital motion) a possible binary manifestation. We also excluded the lowest part in order to avoid the line wings and the blend contributions. The measurements were restricted to the ranges 3–6.5 and 1.35–2.5 of the continuum level for He II λ4686 and He II λ6560, respectively. Finally, instead of Gaussian fitting, we prefer the half-flux method, which measures the wavelength where the selected part of the profile is equally divided with respect to the line flux. Typical results for He II λ4686 and He II λ6560 are shown in the upper part of Figure 10. The semi-amplitude of the variations amounts to $\sim$100 km s^{-1}. In both cases, this is significantly higher than the measurement errors (about 15 km s^{-1}).[5] In the lower part of the figure, we plot the skewness values calculated for the portion of the profile where the velocity measurements were performed (i.e., base and top excluded). We conclude that changes in the line profiles are likely to contribute significantly to the radial velocities changes. Support for this comes from the 1 day recurrence timescale found in the radial velocity curves (upper part of Fig. 10), suggesting that these data do not reflect a $\mathscr{P} = 3.77$ day binary motion. Accordingly, we doubt the reliability of these measurements as a source to derive any eventual orbital parameters.

3.2.1.5. Full-Width at Half-Maximum Variations

In order to measure the full-width at half-maximum (FWHM), we fitted the different lines by a Gaussian profile. For various representative line profile shapes, it was found that the measurements derived by this method correlate very well with the values directly measured on the profile. Typical deviations around the mean value are shown in Figure 11 for selected transitions. Three main conclusions can be drawn from this graph: (a) The semi-amplitude of the variations over one cycle is always quite large (of the order of 100 km s^{-1}). (b) For all lines a clear phase-dependency of the FWHM is found with a 1 day recurrence timescale. N V λ4945 is the only line that does not clearly show this pattern; the latter could be due to the measurement uncertainties, which are considerably higher for this weak line. (c) Slight time delays appear between different lines. We have chosen the phase location of the first maximum as a reference point. In the first group, consisting of He II λ3968 and He II λ4200, this maximum occurs at $\phi \sim 0.1$, whereas for

[5] Unfortunately, the low resolution of the spectra does not allow us to refer to a reliable fiducial mark. Therefore, this quantity was derived from the characteristic dispersion of the measurements for different consecutive exposures.

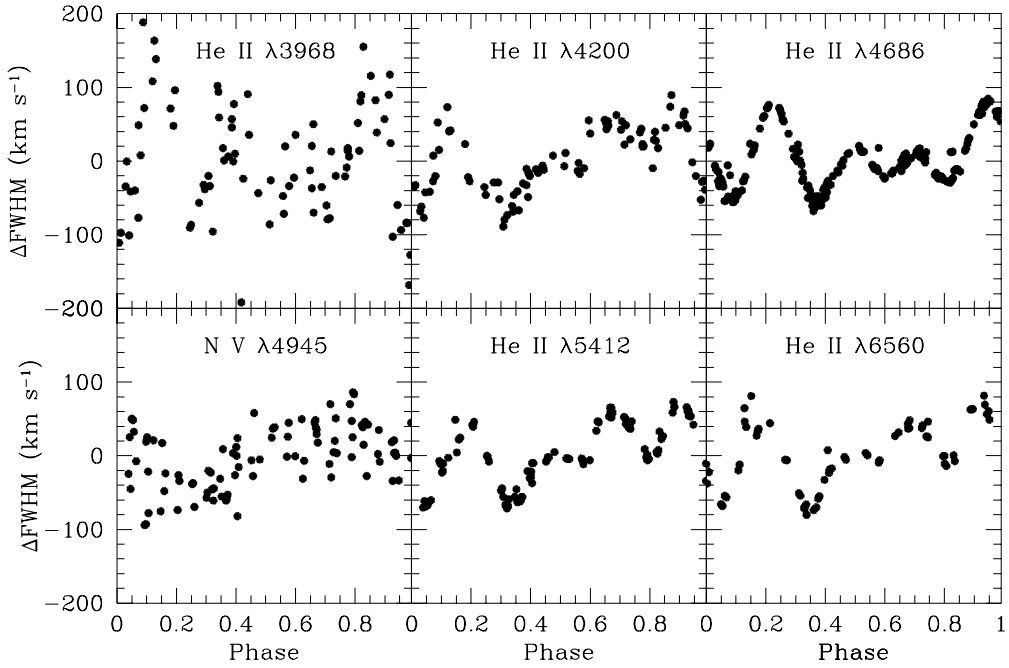

FIG. 11.—Deviations of the full width at half-maximum around the mean value for six selected transitions

the other transitions (He II λ4686, He II λ5412 and He II λ6560) it appears at $\phi \sim 0.2$. The existence of this time delay can be reinforced when one compares the location of the other local extrema for He II λ3968 and He II λ4686. This could be a consequence of the different radial extensions of the line-formation regions in a WR wind (e.g., Niedzielski 1994). In particular, He II λ3968 and He II λ4200 are formed deeper in the wind (maximum emissivity at 3–6 R_c: Hillier 1987; P. Crowther 1995, private communication) than He II λ4686 ($\sim 10\ R_c$: Hillier 1987).

3.2.2. *The P Cygni Profile Variability*

Since the simultaneous UV observations have revealed dramatic changes in the P Cygni absorption components (WRMEGA), we searched for similar *lpv* in the optical P Cygni profiles. Two lines in our sample clearly present a P Cygni absorption component: He I λ3889 and N V λ4604. Also of interest is He I λ5876, but its absorption trough is severely blended with C IV λ5806.

Figure 12*a* presents the temporal behavior of the He I λ3889 absorption component. The variability pattern for this line shares many similarities with N IV λ1718 (WRMEGA). During maximum light, the line develops an enhanced absorption trough at velocities above the estimated wind terminal velocity. Of importance is the fact that the maximum absorption strength at high negative velocities (>2000 km s^{-1}) does not exactly coincides with the variability at intermediate negative velocities (~ 1400 km s^{-1}), as was seen for the UV lines (WRMEGA). Rather, a lack of absorption at this velocity is observed with some delay, at $\phi \sim 0.3$ and 0.55.

Although the bluest part of the He I λ5876 line does not reach the continuum level in EZ CMa, a violet displaced absorption component is clearly seen for WR stars of various subtypes (e.g., Robert 1992). The gross variations affecting the region where C IV λ5806 and He I λ5876 merge are thus most likely related to the variations of this helium absorption trough. The absorption is deepest at light curve maxima (Fig. 12*b*), i.e., at $\phi \sim 0.15$, 0.45 and 0.90, gradually changing its location toward higher velocities, in close resemblance to He I λ3889.

One of the most puzzling characteristics of the present series of spectra is the temporal variations of N V λ4604, which gradually changes from a typical P Cygni profile to a pure emission-line profile on an hourly timescale. As illustrated in Figure 12*c*, a weak absorption trough on the blue side of N V λ4604 appears at $\phi \sim 0.0$ and $\phi \sim 0.5$–0.8. Comparison of Figure 12*c* and Figure 1 shows that the development of this absorption component is completely controlled by the continuum flux variations. This is highlighted in Figure 13, where we show the line intensity at 4588 Å ($v \sim -1025$ km s^{-1}) as a function of phase. Contrary to He I λ3889 and He I λ5876, for which the P Cygni absorption strengthens at maximum light, the weak absorption component in N V appears only as the star fades. The quasi-simultaneous photometric and spectroscopic observations performed by Firmani et al. (1980) led also to the same conclusion. In view of the strong epoch-dependency of the variability in this star, it is remarkable that the same behavior can be noticed in data secured about 20 years ago. A comparison of the spectroscopic data of Smith & Willis (1994) with the photometry performed by Duijsens et al. (1996), both obtained in 1991 January, also supports this tight correlation. A subsequent paper (Morel et al., in preparation) based on a large data set of optical spectra secured over a much longer timescale will further confirm the long-term consistency of this result.

3.2.3. "*Temporal Variance Spectrum*" *Analysis*

As shown in Figure 2, even a simple inspection by eye is sufficient to roughly deduce the temporal behavior of the *lpv*. However, the precise characterization of these varia-

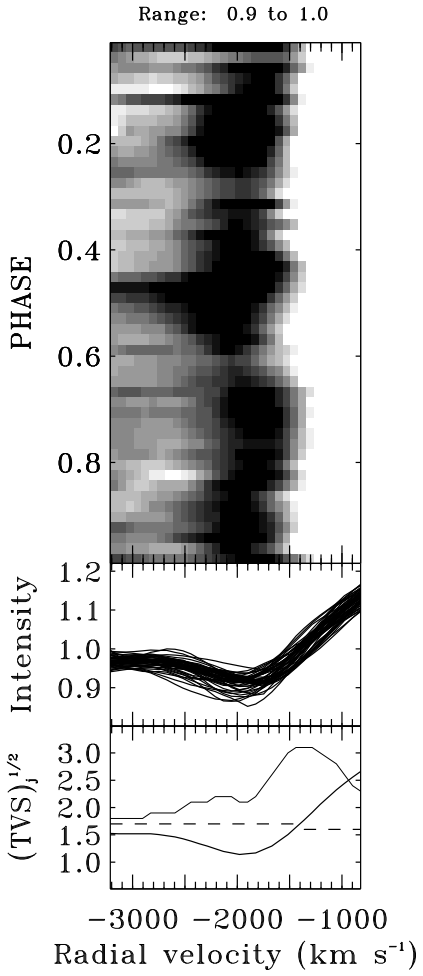

FIG. 12*a*

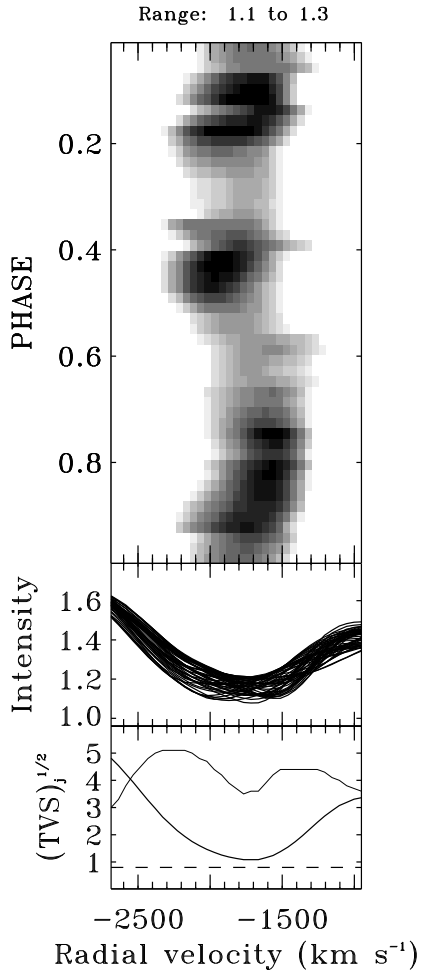

FIG. 12*b*

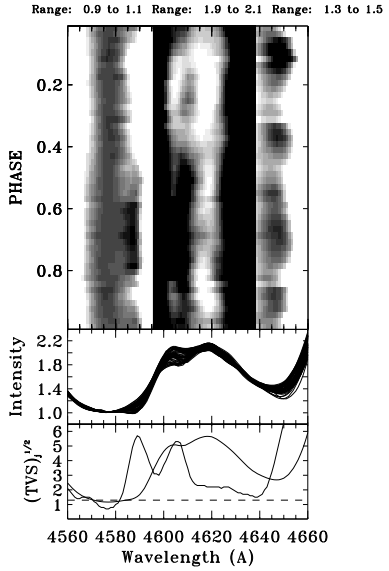

FIG. 12*c*

FIG. 12.—Gray-scale plots of the time series of the P Cygni absorption components of (*a*) He I λ3889, (*b*) He I λ5876, and (*c*) N V λλ4604, 4620. In (*c*), the selected wavelength domain is displayed for three different intensity intervals. The blue wing variability of He II λ4686 is shown at the very right panel of this figure.

tions could be greatly influenced by the photon statistics in the region of interest. In order to rigorously estimate the significance of the *lpv*, we applied the "temporal variance spectrum" analysis (TVS; Fullerton 1990).

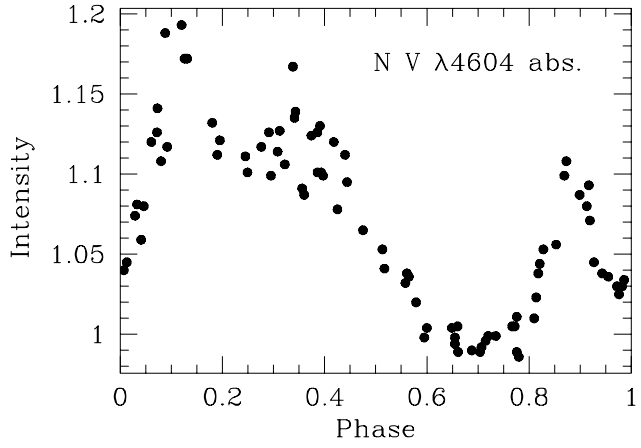

FIG. 13.—Intensity of the N V λ4604 line measured at 4588 Å

In order to describe the *lpv* for a collection of N spectra, we produced a reference spectrum $\bar{S}_j$ as a mean weighted by the signal-to-noise in the continuum associated with each individual exposure. We placed the N rectified spectra in a matrix $S(i, j)$, where i and j denote the spectrum and the pixel (or wavelength bin) numbers, respectively. Then we have calculated the weighted differences:

$$D_{ij} = \left(\frac{\sigma_{0j}}{\sigma_{ij}}\right)(S_{ij} - \bar{S}_j) ,$$

where σ_{0j} is the reciprocal of the rms S/N of the spectral time series (see Fullerton et al. 1996), and σ_{ij} are the elements of the matrix giving the noise associated with the element S_{ij}. In our case, we can reasonably assume that σ_{ij} is given by the Poisson statistics, i.e., by the square root of the count number (in electrons) accumulated at a given pixel. The overall variation for a collection of N spectra will be

$$(\mathrm{TVS})_j = \frac{1}{N-1}\sum_{i=1}^{N} D_{ij}^2 - (\sigma_j^{\mathrm{cal}})^2 ,$$

where $\sigma_j^{\rm cal}$ is introduced in order to eliminate any spurious variability induced by an imperfect wavelength calibration. Following Malanushenko (1988) this quantity can be expressed by the relation:

$$\sigma_j^{\rm cal} = \nabla\bar{S}_j\,\delta_j\,,$$

where $\nabla\bar{S}_j$ is the derivative of the mean spectrum, and δ_j the precision of the wavelength calibration in Å (we have estimated δ_j to be 15 km s^{-1}).

In order to assess the significance of the *lpv*, we compare in the lower panels of Figures 3, 6, and 12 the values of $(\mathrm{TVS})_j^{1/2}$ (expressed in terms of the amplitude of the deviations as a percentage of the normalized continuum) with $[\sigma_{0j}^2 \cdot \chi^2_{N-1}(55\%)]^{1/2}$. Accounting for the noise level in the line profile, any value of $(\mathrm{TVS})_j^{1/2}$ above this threshold ensures that the line-profile variability is significant at the 99% level. An inspection of Figures 3, 6, and 12 shows that this condition is satisfied over the entire profile of all lines (excluding N v λ4945), confirming that the high-velocity variability discussed in § 3.2.1.1 has a physical meaning.

In the following, we will discuss the ratio of $(\mathrm{TVS})_j^{1/2}$ to the mean spectrum (hereafter σ), which allows us to estimate the relative importance of the line-to-line variability. This quantity (*dashed line*, and expressed as the amplitude of the deviations as a percentage of the line intensity at a given wavelength) is overplotted on the mean spectrum in Figure 14. Several characteristics of the *lpv* can be readily deduced from this plot. In particular, the *lpv* create some local maxima of σ along the line profiles. This effect was also noticed for WR 134 by Vreux et al. (1992), and by Robert (1992). Concerning EZ CMa, the same result was found by Robert et al. (1992) for He II λ5412 (see their Fig. 13).

Of interest is the remarkable degree of variability, not only at intermediate to high negative velocities, but also at high positive velocities (Tables 2 and 3). This is particularly noticeable for He II λ4686. Its red wing (around +2140 km s^{-1}; see Table 2) displays an intense peak in the σ spectrum; the size of the deviations amount to ~6% of the line intensity at this velocity.

Since the great majority of optical transitions present a significant level of variability at high positive velocity, it is likely that the red-wing variability of C IV λ5806 affects in some way the variability pattern of the absorption component of He I λ5876 discussed in § 3.2.2. However, mainly

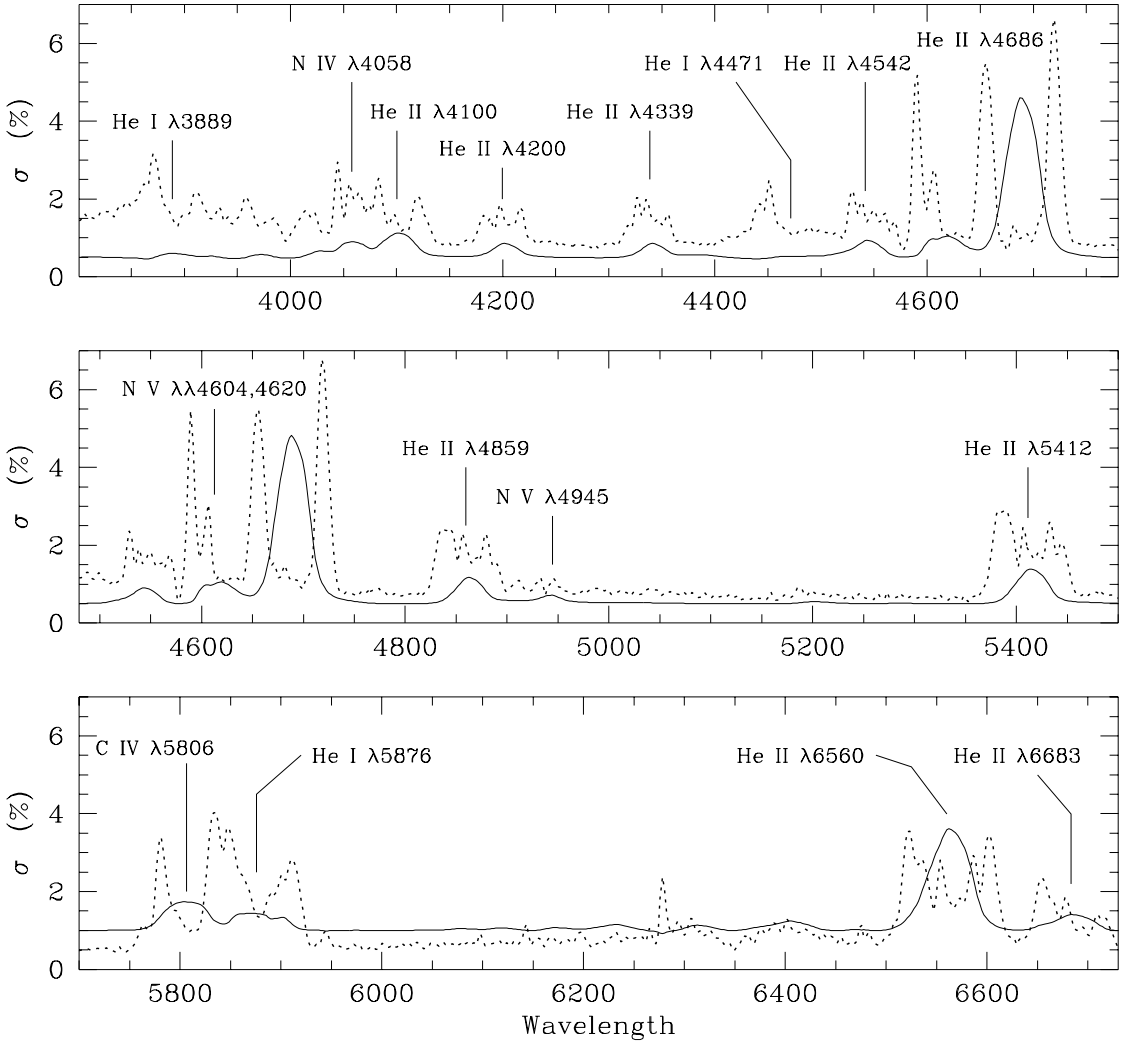

FIG. 14.—Superposition of the σ spectrum (*dashed line*) and the mean spectrum (*solid line*, arbitrary units). Small imperfections of the wavelength calibration lead to spurious peaks at the location of the interstellar and telluric lines (for example around 6279 Å).

TABLE 2

DOPPLER VELOCITIES CORRESPONDING TO THE MAXIMA OF THE TVS FUNCTIONS OF DIFFERENT LINES[a]

N IV λ4058	He II λ4200	He II λ4339	He II λ4542	He II λ4686	He II λ4859	N V λ4945	He II λ5412	C IV λ5806	He II λ6560	He II λ6683
				−1910					−1700	
					−1070		−1270	−1290		−1270
−960	−810	−770	−780			−740				
−140	−130	−170	−200	−260	−120	+60	−230		−260	−230
	+1140	+1120	+1140		+1180		+1160		+1190	
			+1740	+2140			+1800		+1920	

[a] In km s^{-1} and referred to the laboratory rest wavelength (note that the lines may have different "systemic" velocities in a WR wind, e.g., the difference between N V and the He II lines may amount to about 350 km s^{-1} (Smith & Willis 1994).

because of the similarities between the behavior of He I λ5876 and He I λ3889, we believe that the variations intrinsic to the He I absorption trough dominate in Figure 12*c*.

In general, the relative amplitude of the *lpv* is higher for lines formed in the outer part of the wind. This is clearly demonstrated by the decrease of σ along the He II Pickering sequence (Fig. 14). Interestingly, the integral of σ over the extent of a given transition is not correlated with the level of its EW variations (§ 3.2.1.2).

4. DISCUSSION

All our observations point to a strictly coherent phase-dependent behavior of the variability over five consecutive 3.77 day cycles and can be summarized as follows:

1. Extra emission subpeaks are found to travel across all the line profiles (Fig. 3); The bluest excursions of these features coincide with the light curve maxima (Fig. 4).
2. The brightening of the star causes an increase of the EWs, although the amplitude of the EW variations is different from line to line (Fig. 7).
3. A 1 day recurrence timescale within the 3.77 day cycle appears in the FWHM, radial velocities, and skewness measurements (Figs. 9–11).
4. For the He I transitions exposing a blue absorption edge, we observe an enhanced absorption at high velocities at maximum light (Figs. 12*a* and 12*b*).
5. The P Cygni absorption component of N V λ4604 disappears as the star brightens (Fig. 12*c*).
6. There are some zones of enhanced variability along the line profiles (Fig. 14).

For further discussion, we shall refer to the model of the "unperturbed wind," i.e., the wind in (relative) absence of variability. The spectra obtained during the 1983 *IUE* campaign are particularly well suited for the creation of a reference spectrum for the "quiet" wind, since they were obtained during a relatively quiescent stellar state (Willis et al. 1989). Two N IV λ1718 profiles representative of the WRMEGA low and high-velocity states (referring to the blueward extension of the P Cygni absorption components) are compared with the 1983 mean profile in Figure 15. Although some differences are evident, the 1983 profile morphology resembles more the 1995 low-velocity state profile. Therefore, we conclude that the part of the envelope that is seen projected on the stellar disk between $\phi \sim 0.5$ and $\phi \sim 0.8$ is *relatively* unperturbed.

4.1. *A Compact Companion?*

The assumption that the unperturbed wind is related to the minimum of the continuum flux has serious implications for the interpretation of the variability. Indeed, if the perturbations are caused by the presence of a compact companion, the latter would have to be placed in front of the WR star at $\phi \sim 0.1$–0.2 (i.e., at maximum light), as occurs in low-mass X-ray binaries (LMXRB; van Paradijs 1983). Without further advocating the similarity between our case

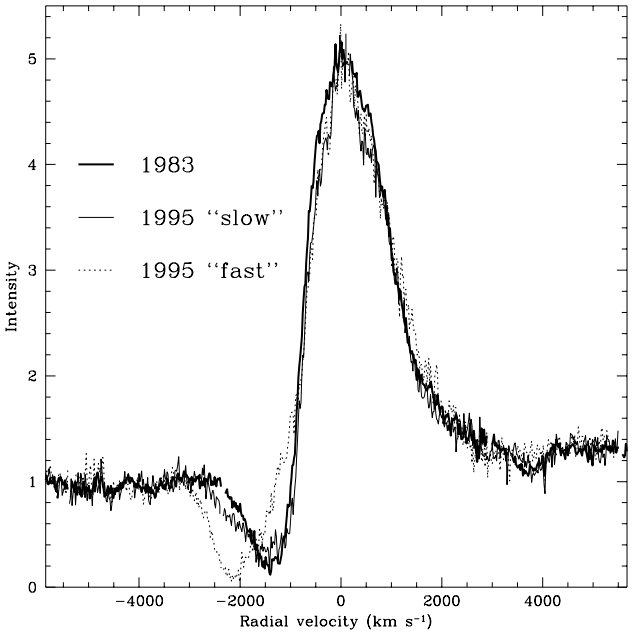

FIG. 15.—Comparison between the representative profiles of N IV λ1718 for the low (*thin line*) and high-velocity states (*dotted line*) as observed by *IUE* in 1995 January, with the one of 1983 September (*thick line*). The 1995 spectra were corrected for the changes of the continuum flux (§ 2.2).

TABLE 3

VELOCITIES OF THE PROMINENT σ SUBPEAKS OBSERVED IN THE P CYGNI ABSORPTION COMPONENTS[a]

N IV λ1718	He I λ3889	He I λ4471	N V λ4604	N V λ4620	He I λ5876
−2300		−1940			−2120
−1100	−1280	−1330	−890	−930	−1380

[a] In km s^{-1} and referred to the laboratory rest wavelength.

and LMXRBs, we discuss below the binary scenario with the hypothetical companion in front at $\phi \sim 0.1$–0.2.

If we assume the presence of a compact companion, we have to explain the simultaneous strengthening of the P Cygni absorption components of the He I transitions and the "evaporation" of the N V λ4604 (and probably N V λ4620) absorption components at $\phi \sim 0.1$–0.5 and $\phi \sim 0.9$. As the ionization cavity around a neutron star crosses the line of sight, one should observe a reduced absorptivity (or emissivity) at intermediate-to-high velocities accompanied by a reduced wind velocity (see § 1). The latter is in complete contradiction to what we observe in EZ CMa: maximum light (hypothetical companion in front) corresponds to maximum wind velocity (WRMEGA and our Fig. 12).

The influence of the hypothetical companion on the EWs of the emission lines strictly depends on the location of the companion's orbit relative to the line formation zones (Marchenko et al. 1996). In general, one expects a minimum in the EWs of the He II (and probably He I) emission lines during the passage of the companion in front of the WR star. This is also not observed in EZ CMa.

Considering the fact that the deepest minimum in the light curve of wind-fed HMXRBs with negligible X-ray heating of the primary (which is expected for EZ CMa because of its low X-ray flux; see below) occurs when the compact companion is in front (e.g., van Paradijs, Hammerschlag-Hensberge, & Zuiderwijk 1978; van Genderen 1981; Pakull et al. 1983), one can argue that the companion is in fact in front at $\phi \sim 0.6$–0.7. This would be consistent with the decrease of the wind velocity at this phase, as well as the decrease of high-speed absorption in He I lines, but cannot account for the appearance of the absorption trough in N V λ4604. Note also that this maximum of N V absorption at $v \sim -900$ km s^{-1} coincides with the maximum emissivity at the same velocity in the N IV and He II lines (Fig. 3). This virtually eliminates the possibility of the companion being in front of the WR star at minimum continuum flux.

The clear indication of the intensity variations at high positive velocities ($v \sim +v_\infty$; Fig. 5) deserves special attention. To quantify them, we have measured the intensity of He II λ4686 and He II λ6560 at the highest positive velocities (v_p) corresponding to the maxima of the TVS functions, together with the intensities at $v \sim -v_p$ in the same spectrum, i.e., at $v = -1910$ and $+2140$ km s^{-1} for He II λ4686, $v = -1700$ and $+1920$ km s^{-1} for He II λ6560 (see Table 2). Both measurements indicate anticorrelated changes with correlation coefficients ranging from -0.44 (He II λ4686) to -0.47 (He II λ6560), i.e., being significant at a greater than 95% statistical level. At first sight, the interpretation is straightforward: the "void" in the WR wind at $v = -v_p$ created by the X-ray source reappears at $v = +v_p$, half an orbital phase later, causing the negative correlation at $v = \pm v_p$. However, there is one fundamental difficulty. Because of the low level of the observed X-ray flux, we expect the zone of the high ionization to be fairly restricted, with an especially well-defined edge at the side facing the densest parts of the wind (i.e., between the ionizing X-ray source and the WR star). This means that the position (in velocity space) of the "void" in the WR wind cannot depend on the line transition. However, we observe significant differences of the maxima of the TVS function at high positive/negative velocities in different lines (Table 2: He II λ6560 vs. He II λ4686). Moreover, the maximum of the TVS for He II λ6560 at -1700 km s^{-1} is placed right at the minimum of the variability of N IV λ1718 (compare with Fig. 3 of WRMEGA). This indicates that the spatial location of the "void" in the WR wind is transition-dependent. This cannot be reconciled with the strictly spatially limited zone shaped by the ionizing X-ray flux from the hypothetical companion.

Since the wind is strongly disrupted between $\phi \sim 0.8$ and $\phi \sim 1.5$ (Fig. 12*c*), the azimuthal extension of the perturbed zone should be very substantial. This may occur if the compact companion is surrounded by a very large photoionized cavity. However, the low X-ray flux of EZ CMa argues against this conclusion. The other possibility is that the compact companion is trailed by some kind of disturbance such as a photoionization wake (Fransson & Fabian 1980), which would suggest some delayed reaction of the profiles. However, this cannot fit the fact that the N V absorption trough vanishes starting from $\phi \sim 0.8$ (Fig. 12*c*), i.e., *long before* the suggested passage of the companion in front of the WR star ($\phi \sim 0.1$–0.2), and once again gains some strength for a short time at $\phi \sim 0.0$ (Fig. 13). Furthermore, the formation of a photoionization wake is only possible for systems with low $\dot{M}/L_X$ ratio (Blondin et al. 1990). Since EZ CMa has a strong wind but is not a strong X-ray emitter, the formation of such a vastly extended structure is very unlikely, additionally owing to the high X-ray opacity of the WR wind.

Other facts are also difficult to account for in the context of the binary hypothesis:

1. The complex and epoch-dependent shape of the light curve is particularly difficult to reconcile with the binary interpretation. Wind-fed HMXRBs are generally characterized by a *stable* double-wave light curve shape, slightly distorted by reflection effects (e.g., Hutchings 1974; van Paradijs et al. 1978; Tjemkes, Zuiderwijk, & van Paradijs 1986). In particular, the occasional complete lack of variations of EZ CMa (Firmani et al. 1980; Duijsens et al. 1996) is not common for HMXRBs. The same conclusion also applies to the polarization curves. The behavior of EZ CMa (Robert et al. 1992) is not typical for HMXRBs (e.g., Dolan & Tapia 1988).

2. A major drawback of the binary scenario arises also from the X-ray observations. The star was below the detection limit of the *UHURU* (2–6 keV) and *HEAO-1* (10–25 keV) satellites, which implies an X-ray luminosity inferior to 1.5×10^{34} and 4.8×10^{33} ergs s^{-1}, respectively (Stevens & Willis 1988). Furthermore, the *ROSAT* and *Einstein* satellites placed an upper limit of 10^{33} ergs s^{-1} on the emissivity in the soft X-ray band (Moffat et al. 1982; Willis et al. 1994). The data can be well described by a thermal spectrum with $kT_X \sim 0.5$ keV. Both L_X and T_X are extremely low compared to any HMXRB (e.g., Haberl, White, & Kallman 1989). This discrepancy might arise from the difference in orbital parameters and stellar wind properties since the amount of material accreted onto a neutron star (and the X-ray luminosity) scales as $F_\star a^{-2} v^{-4}$, where $F_\star$ is the mass flux at the primary's surface, a is the binary separation, and v is the radial outflow velocity at the neutron star location (e.g., Waters et al. 1988). However, detailed calculations have shown that this is not a viable explanation for the observed 2 orders of magnitude deficit (Stevens & Willis 1988). This dichotomy between the X-ray properties of HMXRBs and EZ CMa could then be viewed as significant. We note also that the same calculations applied to other wind-fed

HMXRBs were in reasonable agreement with the X-ray observations (White 1985; Kaper et al. 1993).

This deficiency in the X-ray flux of EZ CMa could be overcome in different ways: (a) The X-ray emission suffers a strong extinction in the dense WR stellar wind (Moffat & Seggewiss 1979). This suggestion was challenged by others (Vanbeveren, van Rensbergen, & de Loore 1982). (b) The accretion is made impossible by centrifugal (or magnetic) inhibition (Stella, White, & Rosner 1986). (c) The conversion of gravitational energy into X-ray emission is much less efficient than usually assumed.

It seems, however, fairly contrived to invoke these mechanisms for which the efficiency is unknown. As for single early-type stars, the X-ray emission could merely be intrinsic to the stellar wind and result from shocks associated with dynamical instabilities (Baum et al. 1992). In short, no firm indication suggests at present that the X-ray emission of EZ CMa is particularly different from that of bona fide single WR stars.

Finally, we question some arguments proposed in support of the duplicity of EZ CMa:

1. Since massive X-ray binaries are believed to be high-velocity objects (van Oijen 1989), it is of interest to determine if EZ CMa is indeed a runaway star. This assertion was first proposed by Moffat (1982), who suggested that its unusual height above the galactic plane for a Population I star ($\sim$315 pc for a distance of 1.8 kpc) arose from a possible recoil after a supernova explosion. However, EZ CMa is certainly dynamically associated with its surrounding ring nebula S 308, as well as with a cavity in the interstellar H I gas (Arnal & Cappa 1996). Since the systemic radial velocity inferred for both objects shows little, if any, departure from the galactic rotation curve at this distance, the status of EZ CMa as a runaway star has since weakened (Chu et al. 1982; Pismis & Quintero 1982; Arnal & Cappa 1996).

2. It was suggested (e.g., Cherepashchuk & Aslanov 1984) that the optical nebulae surrounding some WR stars could be a fossil product of secondary mass exchange in a massive binary system. However, recent hydrodynamical simulations (García-Segura, Langer, & Mac Low 1996) show that this process is not required to reproduce global nebular morphologies, as in the case of S 308.

Could the companion be a main-sequence star? Since its mass should be about solar (Firmani et al. 1980), this implies a very large initial mass ratio, which is unlikely (Garmany, Conti, & Massey 1980). Other arguments such as: the softness of the X-ray emission (see White & Long 1986), the ragged and multipeaked shape of the skewness and radial velocity phase dependencies (see Lewis et al. 1993), and the complicated *lpv* pattern compared to the usual fairly smooth S-wave shape for binary systems seem to reject this possibility.

4.2. *Toward an Interpretation*

All the arguments presented above favor a variability induced by the rotational modulation of an inhomogeneous outflow, as already suggested in WRMEGA. Is it possible in this context to account for points (1)–(6) listed at the beginning of this chapter?

The point that certainly deserves the highest attention is the disappearance of the P Cygni absorption component of N v λ4604 at $\phi \sim 0.1$–0.5. It is worth remembering that this line is formed in close vicinity of the stellar core: the outer boundary of the line formation zone can be put at $r \simeq 10R_c$ for a WN 5 star (Marchenko et al. 1997).

At this point, it might be relevant to examine the variation of the Sobolev line optical depth as a function of radial distance from the star r and azimuthal angle ϕ. For a given transition ($i \rightarrow j$), this quantity can be expressed by the relation ($\mu = 1$):

$$\tau(r, \phi) \sim \left[\frac{n_i(r, \phi)}{g_i} - \frac{n_j(r, \phi)}{g_j}\right] \left| \frac{\partial v(r, \phi)}{\partial r} \right|^{-1} .$$

Depending on the value of the angle ϕ, the line optical depth will be the result of the competition between two quantities—the difference in the population of the atomic levels n_i, n_j, and the radial gradient of the outflow velocity.

Suppose that we observe a "bright" zone of the wind projected on the stellar disk. The only way to produce the disappearance of the nitrogen P Cygni absorption component is either to invoke a steeper velocity gradient in the region where the bulk of emission of N v $\lambda\lambda$4604, 4620 originates and/or to change the population levels. In fact, it is difficult to disentangle the contribution of both effects since the ionization/population balance and the velocity field are intimately linked in the radiation-driven wind theory.

We propose that the increase in the wind temperature occurring at the $\tau \sim \frac{2}{3}$ "surface" at $\phi \sim 0.1$–0.5 (deduced from the color variations of the UV-optical continuum; Fig. 1) leads to a possible rearrangement of the ionization (for N^{3+} and lower stages) as well as the level population balance (overpopulating high levels) in the vicinity of the star. This in turn affects the magnitude of the radiative force since henceforth the new dominant ionic species have their transition wavelengths differently distributed with regard to the maximum of the emergent flux. The resulting changes in the velocity field, combined with a possible altering of the populations of the atomic levels of N^{4+}, cause the replacement of the absorption component of N v λ4604 by emission at $v \sim -900$ km s^{-1}. Concerning the cause of the *lpv* occurring at velocities exceeding the wind terminal velocity, we note that the nitrogen transitions are important contributors to the radiative force acting in hot-star winds (see Table 5 of Abbott 1982). Therefore, a change in the opacity produced by the nitrogen (and possibly iron) ions in the core's vicinity could lead to a redistribution of the momentum deposited by the radiative force throughout the large volume of the wind. In particular, at phases $\phi \sim 0.1$–0.5 (maximum flux), the far-UV transitions that contribute substantially to the flow acceleration might become relatively less opaque. This will lead in turn to an excess of momentum deposited in the remote parts of the wind, and acceleration of the wind beyond v_∞ (compared to the quiet state). Because of this momentum deposition at large radii, the σ spectrum reveals a high level of variability at high velocities (§ 3.2.3; Tables 2 and 3). This could also explain why the transitions formed farther out in the wind (the He II Pickering lines with decreasing principal quantum number) present progressively higher amplitude of variability (§ 3.2.3). Note that the necessity of an additional acceleration of the wind at $v > v_\infty$ was suggested for EZ CMa by Hillier (1988) in order to improve the model fits to the observed profiles.

The morphological changes of the P Cygni absorption components (Figs. 12*a* and 12*b*), can be related to the

pattern of variability in the pure emission lines (Fig. 3). A careful look at Figure 4 shows that an excess of emission appears at $v \sim -1600$ km s^{-1} and $v \sim -2300$ km s^{-1} at $\phi \sim 0.25$, 0.55, 0.90 and 0.15, 0.45, respectively (these velocities are indicated by two dashed lines in this figure). These are roughly the phases when we observe an excess of emission and an enhanced absorption at these velocities in Figures 12*a* and 12*b*. Therefore, the observed P Cygni variability is likely to be due to the motion across the stellar disk of the same zones, which produce the extra emission features on the pure emission-line profiles (Fig. 3). The looplike trajectories of the extra emission components suggest that they are involved in limb-to-center movement induced by the stellar rotation. This is reminiscent of the behavior of the corotating interacting regions in OB stars (Cranmer & Owocki 1996). In this context, note also the gradual increase of the velocity of the extra absorption seen in He I λ5876 (Fig. 12*b*) at $\phi \sim 0.15$, 0.45 and 0.9.

Additionally, we suggest in accordance with St-Louis et al. (1997), that the 1 day recurrence timescale found in the skewness and FWHM measurements highlights the reaction of the wind on the changing conditions at the base of the wind, i.e., on the variable flux emerging from the stellar core.

4.3. *A Hint of a Magnetic Field Structure?*

Our observations of EZ CMa suggest that the wind variability may be induced by some kind of "photospheric" activity such as (non)radial pulsations or magnetic fields. The question of the existence of (non)radial pulsations in WR stars remains open (Vreux 1985; Matthews & Beech 1987). Until now, no ubiquitous observational evidence has been put forward. Although Blecha, Schaller, & Maeder (1992) claimed the existence of a 627 s periodicity in the light curve of the WN 8 star WR 40, subsequent observations carried out by four independent groups were unable to confirm this result (e.g., Martinez et al. 1994).

Some attempts have been made to search for rapid light variations in EZ CMa that could eventually be linked to pulsational instabilities. Moffat & Haupt (1974), Lindgren, Lundström, & Stenholm (1975), and Cherepashchuk (1981) reported the absence of short *periodic* variability (down to 1 hr). Interestingly, such rapid oscillations ($\sim$20 minutes) were reported by Matthews, Moffat, & Marchenko (1992a) and Bratschi & Blecha (1996), but the intermittent nature of this phenomenon (in both cases, once during the entire observation period) makes its interpretation difficult. On the other hand, the uniqueness of the $\mathscr{P} = 3.77$ day period clearly shows up in the intensive photometric monitoring secured by Antokhin et al. (1994). This period seems to be too long for any conceivable (non)radial mode (Glatzel, Kiriakidis, & Fricke 1993).

Matthews et al. (1992a) proposed that the abrupt brightness increase of $\sim$0.008 mag that lasted about 10 minutes in their photometric data may result from a reconnection of magnetic field lines. In that case, the local magnetic field strength would be of the order of 1000 G. Drissen et al. (1989) and Robert et al. (1992) reported a lack of significant circular polarization in broadband continuum, thus excluding cyclotron emission in a large magnetic field, but providing no serious constraints on the possibility of a low magnetic field. McLean et al. (1979) used circular line polarimetry to place a limit of (300 $\pm$ 600) G for the regular component strength. However, it is worth noting that any quantitative estimation of the magnetic field of EZ CMa is loosely constrained since a *local* surface field could easily escape detection (Barker et al. 1981).

From a theoretical standpoint, it is not excluded (but by no means certain) that a local magnetic field with a strength of some hundred G is sufficient to control the wind morphology via creation of magnetically active zones. Although significant attempts have been made to include the effects of a global magnetic field on the wind structure and dynamics (e.g., Friend & McGregor 1984; Cassinelli, Ignace, & Bjorkman 1995), this question remains to be fully addressed theoretically. Such local "photospheric" magnetic activity is susceptible, at least qualitatively, to explain the epoch-dependency and the nature of the variations. We note that the recognition that WR stars could present discrete absorption components (DACs) in their UV resonance lines (Prinja & Smith 1992), as do the majority of O stars, leads to the suggestion that the mechanism inducing the observed variability in both classes of objects is not fundamentally different. It has been suggested (Cranmer & Owocki 1996) that the DAC phenomenon is related to the formation of corotating interacting regions (Hundhausen 1972, chap. 5). These regions emerge from active zones in the stellar photosphere. The development of such large-scale structures is therefore not excluded for EZ CMa. Their curvature induced by the stellar rotation (St-Louis et al. 1997) can introduce small time delays observed in the FWHM variations (§ 3.2.1.5). These structures must be relatively long-lived in order to account for the 5 cycle stability found in our data, as well as for the light curve shape, which can keep the same global pattern on a monthly timescale (Duijsens et al. 1996). In this context, however, the possible existence of magnetic activity for WR stars in conjunction with a presumable lack of surface convective zones remains to be explained.

Another possibility is that the wind of EZ CMa is controlled by a large-scale magnetic structure perhaps of fossil origin (e.g., Brown, Shore, & Sonneborn 1985). We note that an interpretation of the variability of EZ CMa in terms of a bipolar density enhancement was already given by Matthews et al. (1992b). On the other hand, it has been proven that early-type stars can possess complicated magnetic field configuration geometry as a result of the evolution of the fossil field (Thompson & Landstreet 1985). In order to produce the strong-epoch dependency displayed by EZ CMa, this structure should be at some point variable, if not in global morphology, at least in local manifestations.

5. CONCLUSION

Beyond the difficulty of accounting for all the observational aspects presented in this paper, we believe that a relatively coherent picture can be drawn in terms of the rotation of a single WR star with a structured wind. This view is supported by spectropolarimetric studies that emphasized the distorted nature of the wind of EZ CMa (Schulte-Ladbeck et al. 1991, 1992). A contrario, the binary hypothesis hardly finds any support from our observations.

In our interpretation, the variability is induced by the azimuthal dependency of the ionization balance and line opacities prevailing at the base of the outflow. Since the altered opacity modifies the action of the radiative force, the wind is structured in zones differing by their dynamical and physical properties. The streams coming from the active zones at $\phi \sim 0.1$–0.5 and $\phi \sim 0.9$ possess different proper-

ties compared to the ambient wind. As they are carried by stellar rotation, this leads to the complicated pattern of *lpv* seen in our data. This is not surprising, considering the sensitivity of the P Cygni profiles to changes in the wind conditions (e.g., Castor & Lamers 1979; Hamann 1980; Prinja & Howarth 1984).

These observations tend to support the "wind-photosphere connection" for which a growing amount of evidence is now presented for O stars (e.g., Reid & Howarth 1996). Support for this assertion comes from the tight correlation between the changes of the UV continuum flux and spectroscopic variations (WRMEGA; Willis et al. 1989), which signifies that the changes at/near the stellar core drive the wind variability. Although (non)radial pulsations cannot be completely ruled out, magnetic fields are serious candidates for controlling the morphology of EZ CMa's wind. To achieve a complete understanding of the physical processes operating in the envelope of early-type stars, it would be desirable to consider the possible influence of large-scale or localized magnetic field structures on the wind properties. From this point of view, the search for magnetic fields in these objects deserves serious and systematic attention. This could be, for example, accomplished via the detection of circular polarization in very high-resolution and high S/N spectropolarimetric data.

It is a pleasure to thank B. Duffee and F. Mac-Auliffe for their excellent support during this campaign, Paul Crowther for his calculations of the line-formation region of He II λ3968 and N V $\lambda\lambda$4604, 4620 as well as Tony Moffat for discussions and suggestions helping to improve the presentation. We wish to thank the Natural Sciences and Engineering Research Concil (NSERC) of Canada and the Fonds pour la Formation de Chercheurs et l'Aide à la Recherche (FCAR) of Québec for financial support.

REFERENCES

Abbott, D. C. 1982, ApJ, 259, 282
Antokhin, I. I., Bertrand, J.-F., Lamontagne, R., & Moffat, A. F. J. 1994, AJ, 107, 2179
Arnal, E. M., & Cappa, C. E. 1996, MNRAS, 279, 788
Barker, P. K., Landstreet, J. D., Marlborough, J. M., Thompson, I., & Maza, J. 1981, ApJ, 250, 300
Baum, E., Hamann, W.-R., Koesterke, L., & Wessolowski, U. 1992, A&A, 266, 402
Bendat, J. S., & Piersol, A. G. 1986, Random Data Analysis and Measurement Procedures (New York: Wiley)
Blecha, A., Schaller, G., & Maeder, A. 1992, Nature, 360, 320
Blondin, J. M. 1994, ApJ, 435, 756
Blondin, J. M., Kallman, T. R., Fryxell, B. A., & Taam, R. E. 1990, ApJ, 356, 591
Bratschi, P., & Blecha, A. 1996, A&A, 313, 537
Brown, D. N., Shore, S. N., & Sonneborn, G. 1985, AJ, 90, 1354
Cassinelli, J. P., Ignace, R., & Bjorkman, J. E. 1995, in IAU Symp. 163, Wolf-Rayet Stars: Binaries, Colliding Winds, Evolution, ed. K. A. van der Hucht & P. M. Williams (Dordrecht: Kluwer), 191
Castor, J. I., & Lamers, H. J. G. L. M. 1979, ApJS, 39, 481
Chalabaev, A., & Maillard, J. P. 1983, A&A, 127, 279
Cherepashchuk, A. M. 1981, MNRAS, 194, 755
Cherepashchuk, A. M., & Aslanov, A. A. 1984, Ap&SS, 102, 97
Chu, Y.-H., Gull, T. R., Treffers, R. R., Kwitter, K. B., & Troland, T. H. 1982, ApJ, 254, 562
Conti, P. S., Leep, E. M., & Perry, D. N. 1983, ApJ, 268, 228
Cranmer, S. R., & Owocki, S. P. 1996, ApJ, 462, 469
De Donder, E., Vanbeveren, D., & van Bever, J. 1997, A&A, 318, 812
Dolan, J. F., & Tapia, S. 1988, A&A, 202, 124
Drissen, L., Robert, C., Lamontagne, R., Moffat, A. F. J., St-Louis, N., van Weeren, N., & van Genderen, A. M. 1989, ApJ, 343, 426
Duijsens, M. F. J., van der Hucht, K. A., van Genderen, A. M., Schwarz, H. E., Linders, H. P. J., & Kolkman, O. M. 1996, A&AS, 119, 37
Ebbets, D. 1979, PASP, 91, 804
Firmani, C., Koenigsberger, G., Bisiacchi, G. F., Moffat, A. F. J., & Isserstedt, J. 1980, ApJ, 239, 607
Fransson, C., & Fabian, A. C. 1980, A&A, 87, 102
Friend, D. B., & McGregor, K. B. 1984, ApJ, 282, 591
Fullerton, A. W. 1990, Ph.D. thesis, Univ. Toronto
Fullerton, A. W., Gies, D. R., & Bolton, C. T. 1996, ApJS, 103, 475
García-Segura, G., Langer, N., & Mac Low, M.-M. 1996, A&A, 316, 133
Garmany, C. D., Conti, P. S., & Massey, P. 1980, ApJ, 242, 1063
Glatzel, W., Kiriakidis, M., & Fricke, K. J. 1993, MNRAS, 262, L7
Haberl, F., White, N. E., & Kallman, T. R. 1989, ApJ, 343, 409
Hamann, W.-R. 1980, A&A, 84, 342
Hatchett, S., & McCray, R. 1977, ApJ, 211, 552
Henrichs, H. F. 1995, in Multi-Site Continuous Spectroscopy, ed. L. Huang, D. S. Zhai, C. Catala, & B. H. Foing, 11
Hillier, D. J. 1984, ApJ, 280, 744
———. 1987, ApJS, 63, 965
———. 1988, ApJ, 327, 822
———. 1991, A&A, 247, 455
Howarth, I. D., & Phillips, A. P. 1986, MNRAS, 222, 809
Hundhausen, A. J. 1972, Coronal Expansion and Solar Wind (Berlin: Springer)
Hutchings, J. B. 1974, ApJ, 188, 341
Kaper, L., Hammerschlag-Hensberge, G., & van Loon, J. Th. 1993, A&A, 279, 485
Lamontagne, R., Moffat, A. F. J., & Lamarre, A. 1986, AJ, 91, 925
Lewis, D., Moffat, A. F. J., Matthews, J. M., Robert, C., & Marchenko, S. V. 1993, ApJ, 405, 312
Lindgren, H., Lundström, I., & Stenholm, B. 1975, A&A, 44, 219
McCandliss, S. R., Bohannan, B., Robert, C., & Moffat, A. F. J. 1994, Ap&SS, 221, 155
McLean, I. S., Coyne, G. V., Frecker, J. E., & Serkowski, K. 1979, ApJ, 231, L141
Malanushenko, V. P. 1988, Trudu Tartusskoi Astofis. Observatorii, 92, 60
Marchenko, S. V., Antokhin, I. I., Bertrand, J.-F., Lamontagne, R., Moffat, A. F. J., Piceno, A., & Matthews, J. M. 1994, AJ, 108, 678
Marchenko, S. V., Moffat, A. F. J., Eenens, P. R. J., Cardona, O., Echevarria, J., & Hervieux, Y. 1997, ApJ, in press
Marchenko, S. V., Moffat, A. F. J., Lamontagne, R., & Tovmassian, G. H. 1996, ApJ, 461, 386
Martinez, P., Kurtz, D., Ashley, R., & Tripe, P. 1994, Nature, 367, 601
Massa, D., et al. 1995, ApJ, 452, L53
Matthews, J. M., & Beech, M. 1987, ApJ, 313, L25
Matthews, J. M., Moffat, A. F. J., & Marchenko, S. V. 1992a, A&A, 266, 409
Matthews, J. M., St-Louis, N., Moffat, A. F. J., Drissen, L., Koenigsberger, G., Cardona, O., & Niemela, V. S. 1992b, in ASP Conf. Ser. 22, Non-isotropic and Variable Outflows From Stars, ed. L. Drissen, C. Leitherer, & A. Nota (San Francisco: ASP), 130
Moffat, A. F. J. 1982, in IAU Symp. 99, Wolf-Rayet Stars: Observations, Physics, Evolution, ed. C. W. H. de Loore & A. J. Willis (Dordrecht: Kluwer), 263
Moffat, A. F. J., Drissen, L., Lamontagne, R., & Robert, C. 1988, ApJ, 334, 1038
Moffat, A. F. J., Firmani, C., McLean, I. S., & Seggewiss, W. 1982, in IAU Symp. 99, Wolf-Rayet Stars: Observations, Physics, Evolution, ed. C. W. H. de Loore & A. J. Willis (Dordrecht: Kluwer), 577
Moffat, A. F. J., & Haupt, W. 1974, A&A, 32, 435
Moffat, A. F. J., & Seggewiss, W. 1979, A&A, 77, 128
Nichols, J. S., & Fesen, R. A. 1994, A&A, 291, 283
Nichols-Bohlin, J., & Fesen, R. A. 1986, AJ, 92, 642
Niedzielski, A. 1994, A&A, 282, 529
Pakull, M., van Amerongen, S., Bakker, R., & van Paradijs, J. A. 1983, A&A, 122, 79
Pismis, P., & Quintero, A. 1982, in IAU Symp. 99, Wolf-Rayet Stars: Observations, Physics, Evolution, ed. C. W. H. de Loore & A. J. Willis (Dordrecht: Kluwer), 305
Pollock, A. M. T. 1989, ApJ, 347, 409
Prinja, R. K., Barlow, M. J., & Howarth, I. D. 1990, ApJ, 361, 607
Prinja, R. K., & Howarth, I. D. 1984, A&A, 133, 110
Prinja, R. K., & Smith, L. J. 1992, A&A 266, 377
Reid, A. H. N., & Howarth, I. D. 1996, A&A, 311, 616
Robert, C. 1992, Ph.D. thesis, Univ. Montréal
Robert, C., et al. 1992, ApJ, 397, 277
Rochowicz, K., & Niedzielski, A. 1995, Acta Astron., 45, 307
Ross, L. W. 1961, PASP, 73, 354
Schulte-Ladbeck, R. E., Nordsieck, K. H., Taylor, M., Nook, M. A., Bjorkman, K. S., Magalhães, A. M., & Anderson, C. M. 1991, ApJ, 382, 301
Schulte-Ladbeck, R. E., et al. 1992, ApJ, 391, L37
Smith, L. F. 1968, MNRAS, 140, 409
Smith, L. J., & Willis, A. J. 1994, Ap&SS, 221, 189
Stella, L., White, N. E., & Rosner, R. 1986, ApJ, 308, 669
Stevens, I. R., & Willis, A. J. 1988, MNRAS, 234, 783

St-Louis, N. 1994, Ap&SS, 221, 197
St-Louis, N., Dalton, M. J., Howarth, I. D., Willis, A. J., & Conti, P. S. 1997, ApJ, submitted
St-Louis, N., Dalton, M. J., Marchenko, S. V., Moffat, A. F. J., & Willis, A. J. 1995, ApJ, 452, L57 (WRMEGA)
St-Louis, N., Howarth, I. D., Willis, A. J., Stickland, D. J., Smith, L. J., Conti, P. S., & Garmany, C. D. 1993, A&A, 267, 447
Thompson, I. B., & Landstreet, J. D. 1985, ApJ, 289, L9
Tjemkes, S. A., Zuiderwijk, E. J., & van Paradijs, J. 1986, A&A, 154, 77
Tutukov, A. V., & Yungelson, L. R. 1973, Nauch. Inf. Astrosov. Acad. Nauk USSR, 27, 58
Underhill, A. B., & Yang, S. 1991, ApJ, 368, 588
van den Heuvel, E. P. J., & De Loore, C. 1973, A&A, 25, 387
van Genderen, A. M. 1981, A&A, 96, 82
van Kerkwijk, M. H., Geballe, T. R., King, D. L., van der Klis, M., & van Paradijs, J. 1996, A&A, 314, 521
van Oijen, J. G. J. 1989, A&A, 217, 115
van Paradijs, J. A. 1983, in Accretion-Driven Stellar X-Ray Sources, ed. W. H. G. Lewin & E. P. J. van der Heuvel (Cambridge: Cambridge Univ. Press), 189
van Paradijs, J. A., Hammerschlag-Hensberge, G., & Zuiderwijk, F. J. 1978, A&AS, 31, 189
Vanbeveren, D. 1991, Space Sci. Rev., 56, 249
Vanbeveren, D., van Rensbergen, W., & de Loore, C. 1982, A&A, 115, 69
Vreux, J.-M. 1985, PASP, 97, 274
Vreux, J.-M., Gosset, E., Bohannan, B., & Conti, P. S. 1992, A&A, 256, 148
Waters, L. B. F. M., Taylor, A. R., van den Heuvel, E. P. J., Habets, G. M. H. J., & Persi, P. 1988, A&A, 198, 200
White, N. E. 1985, in Interacting Binaries, ed. P. P. Eggleton & J. E. Pringle (Dordrecht: Reidel), 249
White, R. L., & Long, K. S. 1986, ApJ, 310, 832
Willis, A. J., Howarth, I. D., Smith, L. J., Garmany, C. D., & Conti, P. S. 1989, A&AS, 77, 269
Willis, A. J., Schild, H., Howarth, I. D., & Stevens, I. R. 1994, Ap&SS, 221, 321
Willis, A. J., van der Hucht, K. A., Conti, P. S., & Garmany, D. 1986, A&AS, 63, 417

THE ASTROPHYSICAL JOURNAL, 489:1004–1005, 1997 November 10

ERRATUM

In the paper "Optical Spectroscopy of EZ Canis Majoris: Indication for Large-Scale Structures in a Wolf-Rayet Wind" by Thierry Morel, Nicole St-Louis, and Sergey V. Marchenko (ApJ, 482, 470 [1997]), there are several errors that should be corrected. In the legends to Figures 3 and 6 and on page 483, 55% should read 99%. The revised version of Figure 12 given here replaces Figure 12 in the paper.

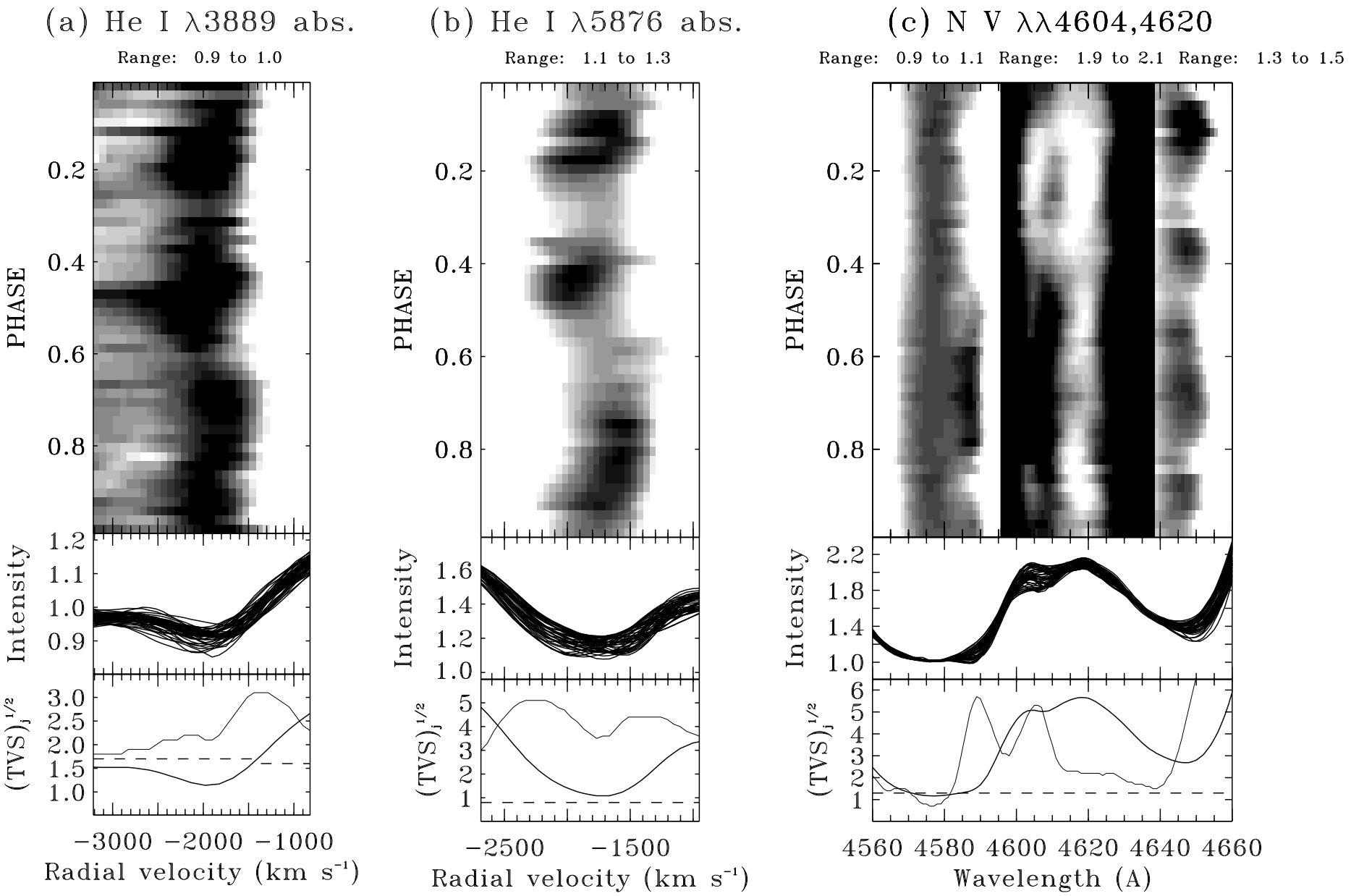

FIG. 12.—Gray-scale plots of the time series of the P Cygni absorption components of (*a*) He I λ3889, (*b*) He I λ5876, and (*c*) N V λλ4604, 4620. In (*c*), the selected wavelength domain is displayed for three different intensity intervals. The blue wing variability of He II λ4686 is shown at the very right panel of this figure.